Phase transitions in systems with frustrated ground states

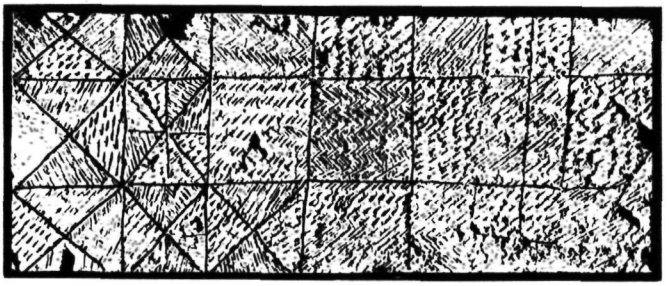

J.M. Thijssen

Phase transitions in systems with frustrated ground states

Afbeelding voorzijde: detail van de absismuur van de abdijkerk van Sénanque (Fr.).

Phase transitions in systems with frustrated ground states

een wetenschappelijke proeve op het gebied van
de natuurwetenschappen,
in het bijzonder de fysica

Proefschrift

ter verkrijging van de graad van doctor
aan de Katholieke Universiteit te Nijmegen,
volgens besluit van het college van decanen
in het openbaar te verdedigen op
donderdag 5 april 1990
des namiddags om 15.30 uur

door

Joseph Marie Thijssen

geboren op 27 februari 1958
te Maastricht

1990

druk: Krips Repro, Meppel

Promotor: **Prof. dr. G. Vertogen**

Copromotor: **Dr. H.J.F. Knops**

Dit proefschrift kwam tot stand met
financiële hulp van de Stichting voor
Fundamenteel Onderzoek der Materie (F.O.M.)

Dankwoord

Het doet mij plezier om op deze plaats allen te kunnen bedanken die op een of andere wijze hebben bijgedragen aan de totstandkoming van dit proefschrift of mij anderszins de afgelopen vier jaar tot een aangename periode hebben gemaakt.

Hubert Knops is voor mij een zeer stimulerende begeleider geweest, die altijd klaarstond om met mij nieuwe resultaten te bespreken of mij verder te helpen als ik problemen tegenkwam. Ik zal altijd een goede herinnering bewaren aan de geanimeerde discussies die we hadden, staande bij het bord op zijn kamer. Verder bedank ik Omar Foda, met wie ik lange tijd de werkkamer heb gedeeld en van wie ik veel over conforme veldentheorie en algebra's heb geleerd. Alle medewerkers van de afdeling theoretische fysica I dank ik voor het aangename gezelschap bij de koffie. Wat betreft de contacten buiten Nijmegen wil ik Hans van Himbergen en Dik Eikmans hier graag bedanken voor hun samenwerking en discussies aangaande de gefrustreerde XY-modellen.

De studenten die ik als docent onder mijn hoede heb gehad bedank ik voor hun bijdrage aan het plezier dat ik aan mijn onderwijstaken heb beleefd en Ap van Gelder voor het aanstekelijke enthousiasme dat hij als mijn collega-assistent aan de dag legde. Ook met Peter Klok heb ik uitstekend samen kunnen werken bij het opzetten en doceren van het college "programmeermethoden".

Het 's avonds thuiskomen was altijd weer een genoegen dankzij Ellen: bij het avondeten vergat ik de beslommeringen van mijn werk altijd weer snel.

Mijn dank gaat ook uit naar mijn ouders; zij hebben mij altijd gestimuleerd om mijn capaciteiten zoveel mogelijk te ontplooien, ook op andere gebieden dan studie en werk.

Contents

Chapter 1

Introduction

In this introductory chapter, I want to give some background to the material covered in this thesis. We will be concerned with models, consisting of stochastic variables, the "particles", on a d-dimensional lattice, where $d = 2$, except for Chapter 2, where d is larger than 2. The Hamiltonian of the system describes the interaction between the particles. In our case these interactions are *frustrated*, which means that there is no configuration for the particles such that all the couplings between them have minimal energy.

This renders the determination of a ground state configuration as a non-trivial task. The ground state is in general degenerate and in particular for models with a discrete symmetry, this degeneration may be quite large. A typical example is the antiferromagnetic Ising model on a triangular lattice, in which it is impossible on any triangle of the lattice to minimize the energy simultaneously on all three bonds.

The degeneracy of the ground state of this model grows with the number of particles as $\exp(Ns_0)$ ($s_>0$, [1]. This example shows that the entropy of a frustrated system may differ from zero at $T = 0$, in violation of the third law of thermodynamics.

1.1 Modulated systems

In a frustrated model, one often finds phase diagrams with a rich structure. This is for example the case in models with modulated phases, that may

occur when the frustration is accompanied by a large degeneration of the ground state. This happens in the ANNNI (axial next-nearest neighbour Ising) model, a variant of the Ising model with in one direction next nearest neighbour interactions of a different sign than the nearest neighbour ones, and in the chiral clock model, a three state model with, again in one direction, competing interactions [2-4]. The latter will be considered in Chapter 2.

A modulated phase is characterized by periodic behavior of the order parameter. If the wave vector of this modulation is commensurate with the lattice constant, one gets a periodic structure with a larger unit cell (supercell). If, on the other hand, the modulation varies continuously with one of the system parameters, one has an infinite unit cell in the generic case, this is called the incommensurate phase. At a phase transition, the wave vector of the modulation may jump from one commensurate value to another, or to an incommensurate behavior.

The archetype models, such as the two mentioned above, have frustration in one dimension in most cases; along the other $d-1$ directions, the couplings are ferromagnetic. Usually, one varies two parameters in such a system, the first of which is the temperature and second one is related to degree of frustration. The phase diagram in this two-dimensional parameter space looks as follows: At $T=0$, one finds two or more commensurate phases, separated by highly degenerate points, from which "fans" , consisting of a large (infinite) number of higher commensurate phases, emerge for $T>0$. At even higher temperatures, there is an onset of incommensurate wedges in between the commensurate regions, until finally the system melts into a high-temperature paramagnetic phase without (modulation) order. When crossing the region below the paramagnetic phase, one finds that the wave vector q varies with the system parameters in a peculiar way: it jumps from one commensurate value to another, and if, occasionally, one crosses an incommensurate region, it varies continuously. It thus forms a "devil's staircase", a complicated structure with self-similarity properties.

This picture has been verified for the ANNNI model [2-4], the chiral clock model [4] and a discrete frustrated ϕ^4 model [5] by means of simulations, low temperature expansions and mean field approximations.

In Chapter 2, we will apply a Migdal-Kadanoff real-space renormalization technique to study the phase diagram of the chiral clock model.

1.2 XY models.

In Chapter 4, 5 and 6, we consider fully frustrated 2-dimensional (2D) XY models. Before describing these models, we will briefly review some properties of the non-frustrated XY model, that will be considered in Chapter 3. An XY model consists of planar spins, i.e. unit vectors in the plane of the lattice, that are characterized by their angle Θ with the X-axis. The interaction is only between nearest neighbour spins and is invariant under global rotations. This nearest neighbour interaction has a unique minimum for equal nearest neighbour spins and no other local minima [6, 7]. This model is a prototype for models described by a fluctuating phase variable. This includes superfluidity and superconductivity where the relevant variable is the phase of the condensate wave function. At low temperature, excitations in this model are spin waves, described by the Gaussian model:

$$\mathcal{H}_{Gauss} = \frac{g}{4\pi} \int_{\boldsymbol{R}^2} (\nabla\Theta)^2$$

At higher temperatures, vortices also come into play, these are endpoints of lines across which the spin angles jump over 2π. The excitation energy of a pair of vortices varies with the logarithm of their distance, just like the Coulomb charges in two dimensions. For a special interaction, the Villain interaction, this model can be shown to be even exactly equivalent to a Coulomb gas (CG). The charges take on the values $+1$ and -1; they live on the dual lattice. The CG Hamiltonian is given by

$$\mathcal{H}_{Coulomb} = \sum_{\mathbf{r_i},\mathbf{r_j}} m(\mathbf{r_i}) m(\mathbf{r_j}) V(\mathbf{r_i} - \mathbf{r_j}) + \mu \sum_{\mathbf{r_i}} m^2(\mathbf{r_i})$$

$$V(r) \approx -\frac{g}{2} \ln(r) \qquad r \to \infty$$

The charges in this Hamiltonian represent the vortices in the original model [6, 7]. The second term on the right hand side controls the abundance of the vortices in the system by a chemical potential μ. For low temperatures, the vortices (or charges) form bound dipole pairs, that give rise to a dielectric constant ϵ. At a certain temperature T_{KT}, these pairs dissociate and $\epsilon \to \infty$., the corresponding transition is called the Kosterlitz-Thouless [8] transition. In the Kosterlitz renormalization theory [9], it is shown that, for $T < T_{KT}$,

the vortices disappear under renormalization, while the Coulomb coupling constant gets replaced by a renormalized value $\tilde{g} = g/\epsilon$. At the transition point, $\tilde{g}/T_{KT}$ takes the universal (i.e. independent of short range details of the interaction and μ) value 4. According to the Kosterlitz theory, the inverse dielectric constant should therefore exhibit at the transition point a *universal* jump from $4T_{KT}/g$ to zero. Kosterlitz-Thouless theory yields a phase diagram in the (T, z) ($z = e^{-\mu/kT}$) plane with a transition line separating the low temperature region, where the charges are bound in pairs and characterized by algebraic decay of correlations, from a high temperature phase where the logarithmic interaction is screened and becomes exponential. The dielectric constant can be directly measured in the XY model, as it is related to the helicity modulus Υ, that is, the second derivative of the free energy to the wave vector q of a twist applied to the spins [10]:

$$\lim_{q \to 0} \epsilon^{-1}(q) = T\Upsilon = T\frac{\partial^2 f}{\partial q^2}$$

In Chapter 3, we discuss a new renormalization theory for the Coulomb gas, developed in 1985 by Minnhagen [11]. This theory predicts a phase diagram with a transition line consisting of two segments. Along the first segment, the dielectric constant jumps from a universal value to zero, however, the second segment is characterized by a nonuniversal jump. The second segment corresponds to higher values of the fugacity z.

We will derive Minnhagen's results by a different procedure than he used, and will be able to reproduce his results in an easier way, giving more insight in the relation with the conventional Kosterlitz renormalization theory.

Next, we turn to the frustrated (FXY) XY models, in which it is no longer possible to obtain a ground state by minimizing all nearest neighbour interactions simultaneously [12-14]. An important application of these models is the description of arrays of superconducting islands, separated by Josephson junctions, in a magnetic field. The planar XY-spins represent the phase of the superconducting wave function in the islands and are thus periodic with period 2π. The coupling via the Josephson junctions is given by the Hamiltonian:

$$\mathcal{H}_{FXY} = J\cos(\Theta_i - \Theta_j + A_{ij})$$

where A_{ij} is connected to the vector potential of the magnetic field through the junction:

$$\sum A_{ij} = \frac{\Phi}{\Phi_0} = 2\pi f$$

where $\Phi_0 = \frac{\hbar c}{2e}$ is the magnetic flux quantum and Φ is the magnetic flux through the junction. The parameter f is called the *frustration.* For $f = p/q$, with p, q integer, it turns out that the ground state is built from $q \times q$ supercells. We restrict ourselves to $f = 1/2$, so $\sum A_{ij} = \pi$. In this case, when calculating the vorticity m on a plaquette, given by $m = \sum (\Theta_i - \Theta_j + A_{ij})$, one finds $(2n+1)\pi$. The ground state consists of vortices $\pm\pi$ that alternate on the lattice, forming a 2×2 unit cell. The $\mathbf{Z}_2$ symmetry of this structure suggests the possibility of an Ising transition. The Ising spins, i.e. the vorticities, reside on the *faces* of the lattice, that is, on the sites of the *dual* lattice.

In addition to this $\mathbf{Z}_2$ symmetry, there is a $U(1)$ symmetry, as in the non frustrated XY model, so one must expect a Kosterlitz-Thouless (KT) transition to occur. Therefore, the question arises wether one can find both KT and Ising transitions in this model and which is their order of occurrence and to what extent can the presence of the one influence the nature of the other.

This question will be studied in Chapter 4, where we map the square lattice frustrated XY model on a Coulomb gas and add an extra Ising interaction to it, to be able to vary the Ising coupling independently from the Coulomb coupling. The subsequent analysis is performed by a Monte Carlo simulation. As it turns out that the order in which the KT and Ising transitions appear may depend on the lattice, a similar analysis is carried out in Chapter 5 for the triangular lattice.

1.3 Conformal field theory

In the last Chapter, we will apply techniques developed in the context of Conformal Field Theory (CFT) [15], to study the frustrated XY model.

Already in the early seventies, Polyakov [16] noted that for critical systems, the Hamiltonian is, in the scaling limit, invariant under conformal transformations of the space. This is a generalization of scaling invariance, which is the basis of the renormalization theory.

Conformal invariance has important consequences for two-dimensional systems, since in that case, the conformal group is infinite dimensional (the conformal group consists then of all analytic functions, with generators z^n), so the invariance leads to an infinite number of conditions on the system. We will restrict ourselves henceforth to $d = 2$. I will not give an overview of the 2D CFT here, but I will simply state some properties of 2D critical theories, that we will need in chapter 6. Some of these properties follow from CFT, others were already known before.

An important conformal mapping in the (complex) plane is

$$z \to \frac{L}{2\pi} \ln z$$

which maps the plane to a strip of width L. In the strip, a transfer matrix $\hat{T} = \exp(-\tau \hat{H})$ acts in the direction along the real axis, called the "time" direction. The partition function for a strip of length N is given in terms of $\hat{T}$ by:

$$Z = Tr(\hat{T}^N)$$

Fields of the theory are in the strip represented by operators. Correlation functions along the strip can be expressed in expectation values of these operators. For a field ϕ:

$$< \phi(\tau, 0)\phi(0, 0) >=< 0|\hat{\phi}(0)e^{-\tau \hat{H})}\hat{\phi}(0)|0 > e^{\tau E_0}$$

In this expression, τ is the coordinate along the strip: the coordinate σ across the strip is taken to be zero. $\hat{\phi}$ is the operator corresponding to ϕ and depends only on σ. E_0 is the ground state of $\hat{H}$ with eigenvector $|0>$, the vacuum.

E_0 is also equal to the free energy (over kT) per unit length along the strip (in excess to the bulk term), it is given by

$$E_0 = -\frac{\pi c}{6\bar{L}}.$$

The number c is called the "central charge" of the theory. Critical exponents x and spin indices l defined for correlation functions of fields in the plane transform under the conformal mapping to the strip into information about the spectrum of $\hat{H}$. In particular, it is found that

$$e^{-\tau \hat{H}}\hat{\phi}(0)|0 >= e^{-2\frac{\pi}{L}(-c/12+\tau x)}\hat{\phi}(0)|0 > \quad \text{as} \quad \tau \to \infty.$$

Most statistical mechanics models correspond to a theory with a unitary transfer matrix. It is one of the important results of the CFT that when such a theory has a central charge $c < 1$, it must be one of the values $c = 1 - 6/[m(m+1)]$, $m = 3, 4, \ldots$. Moreover, all possible exponents x are known once m is given. The Ising model corresponds to $c = 1/2$, $(m = 3)$ and the exponents take on the well known values $x = 0, 1/8$ and 1 for the identity, magnetic field and energy field respectively. The XY and Gaussian model correspond to $c = 1$. Here, no a priory restriction on the exponents is found.

As we saw above, for a model with periodic boundaries on a strip of length τ, one finds the famous formula [17]:

$$F = F_{bulk} - \frac{\pi c}{6L}\tau.$$

Consider now a model with *anti*-periodic boundary conditions on the strip The difference with the periodic case can be extracted form the quotient of partition functions with periodic and anti-periodic boundary conditions, or in the case of the Ising model, the correlation function for two disorder operators [18]:

$$\begin{aligned} e^{F_P - F_{AP}} = \frac{Z_{AP}}{Z_P} &= < \mu(-\tau, 0)\mu(0,0) > \\ &= < 0|\hat{\mu}(0)e^{-\tau \hat{H}}\hat{\mu}(0)|0 > e^{E_0 \tau} = e^{-\frac{2\pi\tau}{L}x} \text{ as } \tau \to \infty \end{aligned}$$

where $x = 1/8$ is the exponent of the disorder operator μ that corresponds via duality to the magnetic operator. In the Gaussian model, a jump of $\Delta\phi = 2q\pi$ across a line along the strip, causes $x = gq^2/2$, the exponent of a spin wave field of charge charge q, to determine the shift in the free energy.

So, by determining the free energy as a function of L, one can calculate the central charge and various exponents in the theory. This is done in Chapter 6 for the frustrated XY model. Use is made of the recently developed Monte Carlo transfer matrix (MCTM) method [19] , by which one can determine the free energy even for systems with continuous degrees of freedom via a transfer matrix formalism.

One of the motivations for doing this, was to verify the conjecture [20], that the $c-$value for the frustrated XY model, when the vortex-unbinding transition and the Ising transition occur simultaneously, be $c = 3/2$. This

would imply that the partition function of the model at the critical point can be written as the product of an Ising and a Gaussian partition function[1] (remember the $c-$values of these models are resp. $1/2$ and 1). This is an example of a *supersymmetric* model. Supersymmetry is the extension of conformal symmetry by a symmetry under the action of an operator with $(x, l) = (3/2, \pm 3/2)$, a so called "chiral current". Supersymmetry implies a special symmetry between bosons (described by the Gaussian free field) and Majorana fermions (described by the Ising model). In string theory, where CFT is of primary importance, supersymmetry plays a major role. For statistical mechanics, supersymmetry implies no special properties for a model at the microscopic level, but it is an appealing idea that supersymmetry may be found in experimental solid state physics.

References

[1] R.M.F. Houtappel, Physica **16**, 1217 (1950).

[2] P. Bak, Rep. Prog. Phys. **45** 587 (1982).

[3] W. Selke, Modulated structures in a simple Ising model, in: *Modulated Structure Materials, T. Tsakalakos, ed.* (Nijhoff, Dordrecht 1984) p. 23.

[4] J.M. Yeomans, in: *Solid State Physics, vol. 41*, H. Ehrenreich, F. Seitz and D. Turnbull, eds (1987).

[5] T. Janssen in: *Incommensurate Phases in Dielectrics, Part one: Fundamentals*, R. Blinc and A.P. Levanyuk, eds. in the series: *Modern Problems in Condensed Matter Sciences*, North-Holland, Amsterdam (1986).

[6] B. Nienhuis, in *Phase Transitions and Critical Phenomena Vol. 11, edited by C. Domb and J.L. Lebowitz* (Academic Press, London, 1987).

[7] J.V. José, L.P. Kadanoff, S. Kirkpatrick, and D.R. Nelson, Phys. Rev. B **16**, 1217 (1977).

[1] On the torus with periodic boundary conditions one can have couplings between the Ising and Gaussian components via the boundary.

[8] J.M. Kosterlitz and D.J. Thouless, J. Phys. C **6**, 1181 (1973).

[9] J.M. Kosterlitz, J. Phys. C **7**, 1046 (1974).

[10] T. Ohta and J.D. Jasnow, Phys. Rev. **B20**, 139 (1979).

[11] P. Minnhagen, Phys. Rev. Lett. **54**, 2351 (1985), Phys. Rev. B **32**, 3088 (1985); P. Minnhagen and M. Wallin, Phys. Rev. B **36**, 5620 (1987).

[12] S. Teitel and C. Jayaprakash, Phys. Rev. **B27**, 598 (1983).

[13] T.C. Halsey, J. Phys. **C18**, 2437 (1985).

[14] S.E. Korshunov and G.V. Uimin, J. Stat. Phys. **43**, 1 (1986); S.E. Korshunov, J. Stat. Phys. **43**, 17 (1986).

[15] A.A. Belavin, A.M. Polyakov and A.B. Zamolodchikov, Nucl. Phys. B **241**, 333 (1984).

[16] A.M. Polyakov, Zh. Eksper. Teor. Fiz. Pis. Red. **12**, 538 [JETP Lett. **12**, 381] (1970).

[17] H.W.J. Blöte, J.L Cardy and M.P. Nightingale, Phys. Rev. Lett. **56**, 742 (1986).

[18] L.P. Kadanoff and H. Ceva, Phys. Rev. B **3**, 3918 (1971).

[19] H.W.J. Blöte and M.P. Nightingale Phys. Rev. Lett. **60**, 1562 (1988).

[20] O. Foda, Nucl. Phys. B **300**, 611 (1988).

Chapter 2

Low temperature renormalization study of the chiral clock model

A new renormalization study for the axial chiral clock model is constructed which refines the one previously presented by Huse by taking the low temperature excitations of the model properly into account. Analysis of the renormalizations equation shows that they yield a correct phase diagram to first order in the low order expansion parameter but still fail to give an accurate description of the phase diagram to higher order.

Published in Physica **143A**, 147 (1987).

2.1 Introduction

In recent years, much attention has been paid to frustrated spin models with highly degenerate groundstates, exhibiting modulated phases [1-3]. Examples of such systems are the ANNNI model [1-4] and the chiral clock model [3, 5].

Phase diagrams of these models appear to be quite complex; the behaviour of the modulation wave vector q as function of a parameter of the system, often exhibits a devil's staircase structure, which means that q assumes an infinite set of rational values [1]. A special characteristic of these devil's staircases in the well-known "self similarity": enlarging the scale of a graph in which q is drawn vs. a relevant system parameter leads to a picture similar to the original graph [1].

This self similarity feature naturally suggests renormalization transformations as a tool to investigate the behaviour of these systems, as these transformations lead to a system with the same topology and interaction structure as the original system by summation over the short range fluctuations, thus regarding the system on a larger scale [6-8].

Some attempts in studying modulated systems by renormalization transformations have been made by Berker *et al.* [9, 10] and Huse [11].

Berker performed a renormalization transformation for Ising spin systems on so-called fractal lattices, artificial structures, unlikely to appear in nature but so designed that a Migdal type renormalization becomes exact.

Huse [11] has studied an asymmetric, or chiral, clock model, i.e. a three state model on a (hyper)cubic lattice of arbitrary dimension with Hamiltonian:

$$H = \sum_{<i,j>} J \cos \frac{2\pi}{3}(\theta_i - \theta_j + \Delta) \tag{1.1}$$

where $\theta_i = 0, 1$ or 2, is the spin on a lattice site i.

Huse used a Migdal-Kadanoff renormalization group method which combines bond shifting with a decimation procedure [12, 13]. Although quite complex phase diagrams including self similar structures have been found by Huse, there remain important discrepancies with the results from low temperature expansions performed by Yeomans and Fisher [14-16] for the axial chiral Potts model (see below).
The most important differences are:

- In the renormalization study, first-order transitions between the various phases do not occur, in contradiction with low temperature expansions.
- The modulation vectors found by Huse do not correspond with those found by Yeomans and Fisher, also, the devil's staircase found by Huse, is different from the "devil's top step" found in low temperature expansions, where the q-values become densely spaced only at the edge of the modulated region.
- Contrary to the low temperature expansion, Huse finds a strong dimensional dependence of the structure of the phase diagram. This may be a consequence of the fact that he studied a model with chiral interactions in *all* directions.

In this article we want to explore to what extent it is possible to improve on the renormalization picture of Huse especially in the low temperature region where comparison with the exact results of Yeomans and Fisher is possible. In order to do this we study the axial version of the chiral clock model. The low temperature behaviour of this model can (for $d > 2$) be understood from spin excitations in homogeneous layers [16]. We set up a renormalization transformation that takes these excitations into account to first order in the temperature expansion parameter.

In section 2, the renormalization equations are derived. Section 3 contains the phase diagrams resulting from these equations.

2.2 The renormalization equations

We study an axial chiral clock model [11], consisting of a large number (N) of $d-1$ dimensional layers.

In the layers, the 3-state spins are ferromagnetically coupled by a Potts interaction. The interaction between the layers is asymmetric. The hamiltonian reads:

$$H = J^{\parallel} \sum_{<i,j>}{}^{\parallel} \cos\frac{2\pi}{3}(\theta_i - \theta_j + \Delta) + J^{\perp} \sum_{<j,m>}{}^{\perp} \delta_{\theta_j,\theta_m} + const. \qquad (2.1)$$

We define the Boltzmann weights

$$X = Ae^{\beta J^{\parallel} cos 2\pi \Delta/3}, \qquad Y = Ae^{\beta J^{\parallel} cos 2\pi(1-\Delta)/3}$$

and (2.2)

$$Z = Ae^{\beta J^{\parallel} cos 2\pi(1+\Delta)/3}.$$

The constant A can be fixed by the requirement $X + Y + Z = 1$. Note the difference with the system studied by Huse, in which there are asymmetric clock couplings in all directions.

We assume the bonds *in* the layers to be strong, the weight $w \equiv e^{-q_\perp J_\perp}$ of a spin flip in a homogeneous layer is the low temperature expansion parameter, with $q_\perp = 2(d-1)$ is the number of nearest neighbours of spins *in* the layers.

The bonds between the layers can have arbitrary values, however, in the regions of interest, i.e. close to the multi-phase point (e.g. $X \approx Y$), these bonds often appear to be weak. In the usual Migdal Kadanoff renormalization bonds are shifted in such a way that all but a fraction l^{-d} of the spins can easily be summed out. This procedure is not too bad an approximation when (*i*) the shifted bonds are weak as the error made is second order in the bond strength [13]; (*ii*) the shifted bonds are strong but are shifted in an environment of ferromagnetic bonds of the same strength enforcing almost all spins to have the same sign. Indeed, the Migdal transformation yields the right thermal exponent $y_T = d - 1$ [1] for the zero temperature fixed point. The disadvantage of the Migdal Kadanoff transformation is that, although the free energy is given correctly to zeroth order in w [17], it deviates from the right value already in first order in w. In the present case of the axial chiral clock model these results imply that it is still reasonable to shift the strong $J^\perp$ bonds within a layer but that one should avoid shifting them between layers since these may be weakly coupled. As a first step in deriving the renormalization equations we notice that in the low temperature regime the majority of the spins in each layer $j = 1,..,N$ have the same value θ_j, with to order w only isolated excitations $\theta_j \pm 1$. (corresponding to the domain wall excitations of Yeomans and Fisher). Summing out these excitations leads to an effective triplet interaction $E(\theta_{i-1}, \theta_i, \theta_{i+1})$ due to the fact that the weight of an excitation depends (via the chiral bonds) on the value of the majority spin in the two neighbouring layers. The triplet

[1] One can verify this by considering two neighbouring cells of a d-dimensional Potts system. Such cells interact via l^{d-1} bonds, where l is the renormalization constant, so that the new interaction parameter J' becomes $J' = l^{d-1}J$, so $\lambda = l^{d-1}$.

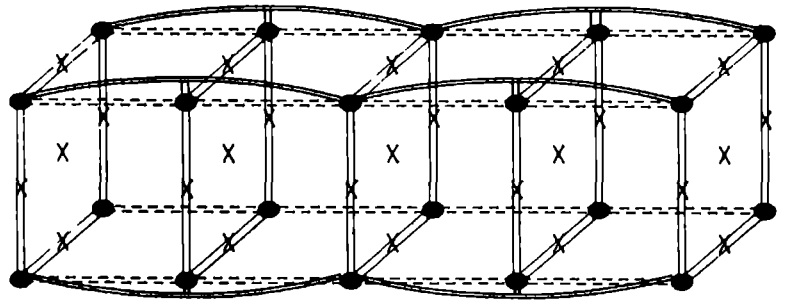

Figure 1: Bond structure in the chiral clock model after performing the bond shifting procedure described in the text. The 'x'-spins are summed over; the solid circles represent the remaining spins in the lattice.

interaction is easily found to be:

$$\begin{aligned} E(0,0,0) &= \ln(1+2w\frac{YZ}{X^2}) \approx 2w\frac{YZ}{X^2} \\ \left.\begin{matrix} E(0,1,0) \\ E(0,2,0) \end{matrix}\right\} &= \ln\left[1+w(1+\frac{X^2}{YZ})\right] \approx w(1+\frac{X^2}{YZ}) \end{aligned} \qquad (2.3)$$

while the interaction for all other 24 triple configurations follow by symmetry. Notice that this interaction is a weak interaction of order w. In the next step we shift interactions taking care of the rules explained above. According to these rules only the weak triplet interaction can be shifted in all directions while all two spins interactions may only be shifted in transverse directions. Using this freedom one can arrive at a bond structure as shown in Fig. 1. Counting the number of shifted bonds shows that the chiral bonds become $p \equiv 2^{d-1}$ times as strong so that the corresponding Boltzmann weights X, Y, Z should be replaced by X^p, Y^p and Z^p. The triple bonds which have been shifted both in transverse and in axial directions become $2p$ times their original strength while the transverse coupling $J^\perp$ is multiplied with a factor $1/2p$. In the last step one carries out a decimation by summing over all spins indicated by crosses in Fig. 1. For the spins not connected by axial bonds this sum leads to a renormalized value of the transverse coupling $w' = e^{-2(d-1)J'^\perp}$, which is the same as the usual Migdal expression and is

given by:

$$e^{-J'_\perp} = \frac{2e^{-(p/2)J_\perp} + e^{-pJ_\perp}}{1 + 2e^{-pJ_\perp}}. \tag{2.4}$$

For all dimensions that we will consider, w has attractive fixed points at $w = 0$ and $w = 1$ and a repulsive one between 0 and 1. Thus the starting value for w should lie between zero and the repulsive fixed point value.

As a last step, we have to sum over the remaining spins in the odd-numbered layers. Here we do not find the usual Migdal expression as these spins are connected both by chiral bonds in the axial directions and by ferromagnetic bonds in the transverse direction. However, in a low temperature expansion the sum is still easy to carry out. Recall that the layer excitations are correctly represented to order w by the triple interactions. So to this order we can safely neglect the layer excitations. The Boltzmann weight corresponding to the renormalized chiral bond between two even layers is then simply found by summing over the three possible spin values of the odd layer in between. For example one finds for $\theta_0 = 0$ and $\theta_2 = 0$:

$$\tilde{X}^L = X^{2pL} e^{2pLE(0,0,0)} + Y^{pL} Z^{pL} e^{2pLE(0,1,0)} + Y^{pL} Z^{pL} e^{2pLE(0,2,0)} \tag{2.5}$$

where L is the number of spins left in a layer. In the limit $L \to \infty$, $\tilde{X}$ is determined by the largest of the three terms in the right hand side and one finds using (2.3):

$$\begin{aligned} \tilde{X} &= \max\{X^{2p} e^{4pw\, YZ/X^2}, (YZ)^p\, e^{2pw(1+X^2/YZ)}\} \\ &\approx \max\{X^{2p}(1 + 4pw\frac{YZ}{X^2}, (YZ)^p(1 + 2pw(1 + \frac{X^2}{YZ}))\}. \end{aligned} \tag{2.6a}$$

In the same way one obtains

$$\tilde{Y} = \max\{Z^{2p}(1 + 4pw\frac{XZ}{Z^2}), (XY)^p(1 + 2pw(1 + \frac{Z^2}{XY}))\} \tag{2.6b}$$

$$\tilde{Z} = \max\{Y^{2p}(1 + 4pw\frac{XZ}{Y^2}), (XZ)^p(1 + 2pw(1 + \frac{Y^2}{XZ}))\}\,. \tag{2.6c}$$

The final renormalized Boltzmann weights are obtained by extracting a normalization constant:

$$X' = \tilde{X}/(\tilde{X}+\tilde{Y}+\tilde{Z}), \quad Y' = \tilde{Y}/(\tilde{X}+\tilde{Y}+\tilde{Z}), \quad Z' = \tilde{Z}/(\tilde{X}+\tilde{Y}+\tilde{Z}). \tag{2.7}$$

The most conspicuous difference of these renormalization transformations with those of Huse is the fact that they are not analytic at the lines at which the two terms, of which the maximum determines $\tilde{X}$, (respectively $\tilde{Y}$ and $\tilde{Z}$) cross. These lines are found to be given by the equations:

$$X^2 = YZ, \quad Z^2 = XY, \quad Y^2 = XZ\ . \tag{2.8}$$

In the sequel we will find it convenient to represent, following Huse [11], the Boltzmann weights X, Y and Z by a complex number λ defined as

$$\lambda = X + e^{2\pi\imath/3}Y + e^{-2\pi\imath/3}Z \tag{2.9}$$

The fact that $0 \leq X, Y, Z \leq 1$ and $X+Y+Z = 1$ confines λ to an equilateral triangle [Fig. 2]. The points A,B,C in this figure correspond respectively to the ferromagnetic point $X = 1$, $Y = 0$, $Z = 0$; and the points $X = 0$, $Y = 1$, $Z = 0$ and $X = 0$, $Y = 0$, $Z = 1$ belonging to the chiral and anti-chiral groundstates. The point P with $X = Z = Y = 1/3$ is the point where the layers are decoupled. Also drawn in Fig. 2 are the lines $X^2 = YZ$ etc., we see that they divide the triangle in six regions inside each of which the renormalization equations are analytic.

2.3 Analysis of the renormalization equations

In this section, we will study the renormalization equations and give the phase diagrams resulting from them.

One can verify from Eqs. (2.6) that the points A and P are fixed points of the transformation and B and C form a fixed cycle of order two, i.e. B goes over in C under the transformation and vice versa.

A and the fixed cycle BC are attractive for λ small enough whereas P has one eigenvalue equal to zero, and one positive. To identify the modulation vector of the various phases, we follow the method described by Huse [11]. He observed, that the two point correlation function G, defined as

$$G(\mathbf{r}_i, \mathbf{r}_j) \equiv < \exp\left(\frac{2\pi i}{3}(\theta_{\mathbf{r}_i} - \theta_{\mathbf{r}_j}\right) > \tag{3.1}$$

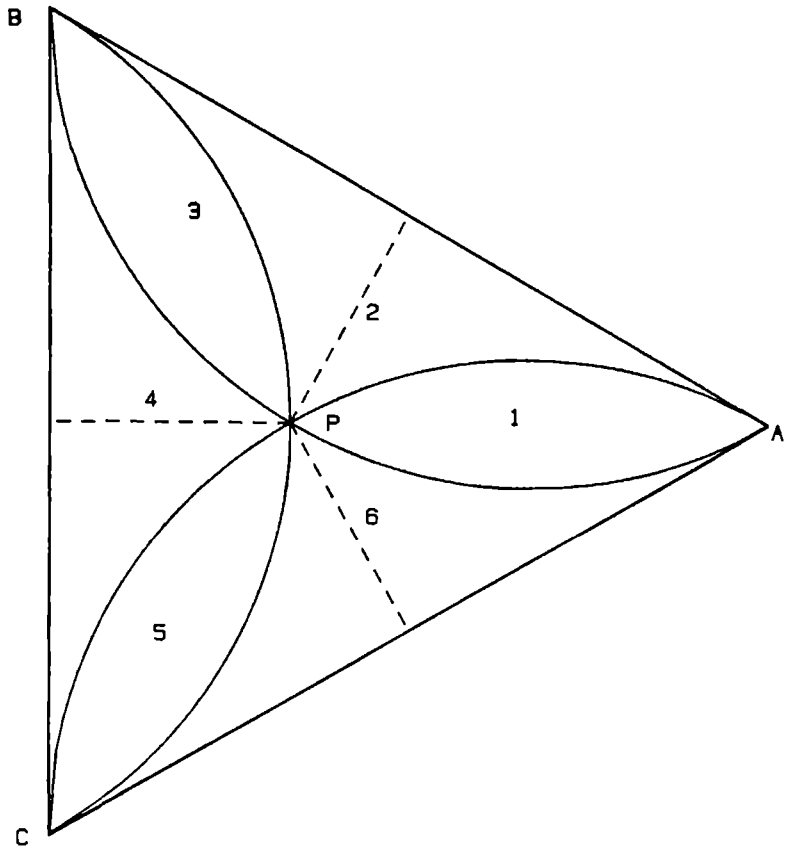

Figure 2: The 'λ-triangle'. Solid lines represent the borders at which the renormalization equations (2.6) are non-analytic.

obeys the following symmetry relation:

$$G(\mathbf{r}_n, \mathbf{r}_m; \lambda e^{2\pi i/3}) = G(\mathbf{r}_n, \mathbf{r}_m; \lambda) e^{2\pi i(m-n)/3} \tag{3.2}$$

where m and n denote the mth and nth layer respectively. Together with the symmetry property that G changes into G^* if we interchange Y and Z ($\lambda \rightarrow \lambda^*$):

$$G(\mathbf{r}_i, \mathbf{r}_j, \lambda) = G^*(\mathbf{r}_i, \mathbf{r}_j, \lambda^*) \tag{3.3}$$

this yields a six-fold symmetry. Now it is expected, that the correlation function is, at least asymptotically, given by

$$G(\mathbf{r}_n, \mathbf{r}_m, \lambda) = A(\mathbf{r}_n, \mathbf{r}_m) e^{2\pi i(m-n)q(\lambda)} \tag{3.4}$$

with A real. The parameter $q(\lambda)$ defines the modulation vector which is axially directed.

From the symmetries Eqs. (3.2) and (3.3) it follows that the value of q is known at the symmetry lines $\arg(\lambda) = 2\pi n/6$ $n = 0, 1, \ldots, 5$ to be $q = n/6$. Notice that these symmetry lines divide the λ-triangle in six segments.

Following Huse, we now assume a "weak monotonicity" property demanding that the value of $q(\lambda)$, for λ in a given segment, is located between its values at the boundaries of the segment, in formula:

$$\begin{aligned} &\text{when} \quad 2\pi n/6 \leq \arg(\lambda) < 2\pi(n+1)/6 \\ &\text{then} \quad n/6 \leq q(\lambda) < (n+1)/6. \end{aligned} \tag{3.5}$$

The renormalization group transformations are set up in such a way, that with each step, $q \rightarrow 2q$ (mod 1).

From the properties of $q(\lambda)$, considered above, we see that in the fixed point A, $q = 0$, corresponding to ferromagnetic order, whereas in B, $q = 1/3$ and in C: $q = 2/3$, corresponding to perfect chiral (anti-chiral) order.

Apart from the separation lines between the various phases, which map after many transformations onto the para-fixed point P, any starting point in the triangle will, after a number of transformations, end up in one of the corners of the triangle, where q is known. A point close to A, where $q = 0$, moves towards A. A point close to B (where $q = 1/3$) changes into a point close to C, as $q' = 2q = 2/3$. After another iteration, $q' = 2q =$

$2 \cdot 2/3 \bmod 1 = 1/3$, so we are again near B. Because the fixed cycle BC is attractive, the point will move closer and closer to BC.

We determine the q of a point in the triangle by "walking back" to it from the corner where that point ends up after a number of transformations, keeping track of q at each step. Note that the property $q' = 2q \bmod 1$, where q' is the image of q after one transformation, gives, in walking back, two possibilities for every new q, namely $q = q'/2$ or $q = (q' + 1)/2$. However, using (3.5), we can easily make the choice between the two. The q values found in this way form the set $q = m/2^n \cdot 3$.

Huse finds above a critical dimension also fixed cycles of higher order; allowing eventually all rational values for the modulation vector q. The present equations do not yield such cycles.

We will turn now to the phase diagrams. First we show that the renormalization equations (2.6), (2.7) and (2.4) yield to first order in w the same phase diagram as found by Yeomans and Fisher.

2.3.1 First order in w

We will discard all effects of order higher than w, which means, that after one transformation, w', which is of order $w^{p/2}$, is set equal to zero.

We first study the phase diagram for $w = 0$. The following properties are then found.

- region 2 [see Fig. 2] is after one transformation mapped onto the line $Y^2 = XZ$. The line segment $X = Y$, $Z < 1/3$ maps onto the para-fixed point P. Regions 4 and 6 transform in a similar way.

- The line $Y^2 = XZ$, $X > 1/3$ is invariant under the transformation; points on it move to A.

- Within the fish shaped region (1), points move to A. Points in (3) move to (5) and vice-versa, until the points B and C are reached.

From these facts, one can conclude that the phase diagram consists of three regions: $X > Y, Z$ has $q = 0$; $Y > Z, X$ has $q = 1/3$ and for $Z > Y, X$, one finds $q = 2/3$.

The different phases are separated by first order transition lines. This follows from a direct iteration of the recursion relation for the free energy.

Using the homogeneity of the renormalization equations, one finds:

$$f(X,Y,Z) = l^{-nd} \ln(\tilde{X}_n + \tilde{Y}_n + \tilde{Z}_n) + l^{-nd} f(X'_n, Y'_n, Z'_n) \qquad (3.6)$$

where $\tilde{X}_n$ and X'_n etc. denote the n-fold iterates of Eq. (2.6) resp. (2.7). Since X'_n, Y'_n and Z'_n are properly normalised, the free energy in the right hand side remains bounded and one has:

$$f(X,Y,Z) = \lim_{n\to\infty} l^{-nd} \ln(\tilde{X}_n + \tilde{Y}_n + \tilde{Z}_n). \qquad (3.7)$$

Now consider a point of the phase diagram which initially has $X > Y, Z$. As shown above, such a point is attracted, at least to zeroth order in w, by the fixed point A, i.e.

$$\lim_{n\to\infty} X'_n = 1, \quad \lim_{n\to\infty} Y'_n = 0, \quad \lim_{n\to\infty} Z'_n = 0. \qquad (3.8)$$

It follows also, that

$$\lim_{n\to\infty} \tilde{Y}_n/\tilde{X}_n = 0, \quad \lim_{n\to\infty} \tilde{Z}_n/\tilde{X}_n = 0 \qquad (3.9)$$

and one concludes:

$$f(X,Y,Z) = \lim_{n\to\infty} l^{-nd} \ln \tilde{X}_n \ . \qquad (3.10)$$

To zeroth order in w, $\tilde{X}$ is simply given by

$$\tilde{X} \ = \ X^{2p}$$

(when $X > Y, Z$), from which it follows, that

$$\tilde{X}_n \ = \ (X^{2p})^n \ . \qquad (3.11)$$

Inserting this relation in Eq. (3.8) and noting that the rescaling length l is equal to 2 and that p is defined as $p = 2^{d-1}$ yields finally:

$$f(X,Y,Z) = \ln X \qquad X > Y, Z \ . \qquad (3.12)$$

A similar reasoning for the other two regions gives

$$f(X,Y,Z) = \ln Y \text{ for } Y > X, Z; \quad f(X,Y,Z) = \ln Z \text{ for } Z > X, Y \ . \qquad (3.13)$$

From these explicit formulae, it is clear that the lines $X = Y$, $X = Z$ and $Y = Z$ are first order transition lines.

It should be noted that the first order transitions obtained from the present renormalization transformation do *not* result as usual [18] from the presence of a fixed point with eigenvalue l^d (the para-fixed point, which separates the phases, has

$$\lambda = \frac{p - 6p\lambda + 4p^2 w}{1 + 4p\lambda}$$

as eigenvalue). The first order transition in the present case must be attributed to the non-analytic structure of the renormalization equations around the para-fixed point.

The phase diagram in first order in w is found by a study of the iterated renormalization equations where all higher order terms in w are neglected.

In view of Eq. (2.4) this means that only in the first step the full equations (2.6) should be used, while in all further steps one has effectively $w' = 0$. As the q-values of the phases that result from these further steps have just been evaluated, this analysis is simple.

It turns out that there is a wedge-shaped region around the line segment $Y = Z$, $X < 1/3$, extending from the para-point P to the edge $X = 0$, that is mapped onto the region $X > Y, Z$ in the first transformation.

Because $w = 0$ after the first step, these points will then, under subsequent transformations, move to A, where $q = 0$. The procedure for finding q, described above, assures us that in this wedge-shaped region around $Y = Z$, $q = 1/2$. There are similar wedges around $Y = X$, $Z < 1/3$ and $X = Z$, $Y < 1/3$ that are mapped onto $Y > X, Z$ and $Z > X, Y$ respectively, [see Fig. 3] and one can verify that the associated q-values are $q = 1/6$ and $q = 5/6$.

The regions between the wedges have $q = 0$, $1/3$ or $2/3$. So we find six different q-values in first order. The phases found correspond precisely to those obtained by Yeomans and Fisher in first order. The phase boundary, e.g. between the $q = 1/3$ and $q = 1/6$ phase, follows from the condition $\tilde{Y} = \tilde{Z}$, hence it is given by:

$$Y/X - 1 = 2w(\frac{Z^2}{XY} + 1 - 2\frac{XZ}{Y^2}) \tag{3.14}$$

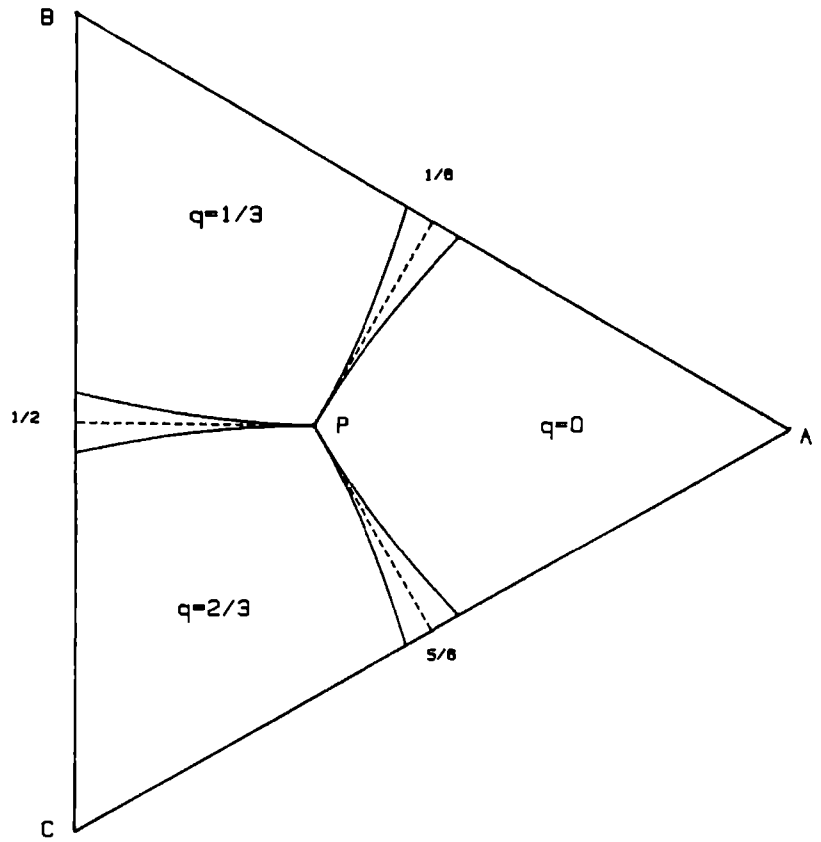

Figure 3: First order phase diagram. Wedges correspond to $q = 1/6$, $q = 1/2$ and $q = 5/6$. The borderlines of these phases are first order transition lines.

which is in accordance with the formula found by Yeomans and Fisher to first order in w. The first order character of the transition between the phases is conserved, because the borderlines of the phases are mapped onto the first order lines obtained above. We can conclude that the first order approximation in w gives results in agreement with low temperature expansions.

2.3.2 General order in w

Having established that the renormalization transformation Eqs. (2.4), (2.6) and (2.7) properly represents the phase diagram to first order in w, we now turn to the analysis of the full equations in order to see which features of the low temperature phase obtained by Yeomans and Fisher are reproduced. One should note, however, that the renormalization equations (2.6) are correct only to first order in w.

We first notice that the dimensionality, which enters our equations via the value of $p = 2^{d-1}$, does not influence (in accordance with Yeomans and Fisher) the phase diagram in an essential way. The reason is that the eigenvalue

$$\lambda = \frac{p - 6pw + 4p^2w}{1 + 4pw}$$

remains relevant for $d > 2$.

In our numerical analysis we further take $d = 4$, and an initial value for $w = 0.6$ (i.e. close to the fixed point value of Eq. (2.4)), which values are chosen so that a fair amount of the complex structure of the phase diagram can be resolved in the numerical analysis.

The most important new phases are represented in Fig. 4a, which is a schematic diagram, and only used to elucidate the structure of the new diagram. Despite the apparent simplicity of the figure, the phase structure has become much more complicated with respect to Fig. 3. There are again regions around the lines $X = Y$, $Z < 1/3$ etc. corresponding to $q = 1/6$, $1/2$ and $5/6$ as in the first order case. However, there is, between the $q = 1/6$ and $q = 1/3$ phase, a wedge that is mapped on the $q = 1/2$ region after one transformation. This wedge must thus be identified as the $q = 1/6$ phase. Between the $q = 1/4$ phase and the $q = 1/6$ phase there is again a wedge that is mapped on a wedge between the $q = 1/3$ and $q = 1/2$ phase after one transformation and on the $q = 5/6$ phase after two transformations. This

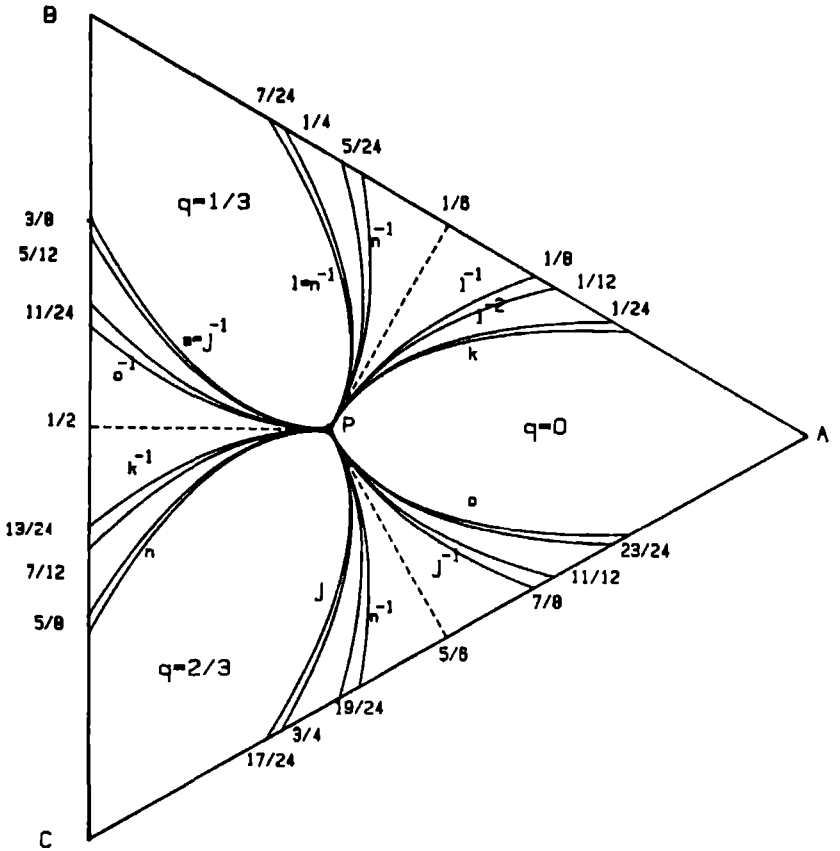

Figure 4: Phase diagram for arbitrary order in w. a: schematic diagram (b): the realistic diagram for $d = 4$, $w = 0.6$. All the separation lines shown consist of an infinite number of phases.

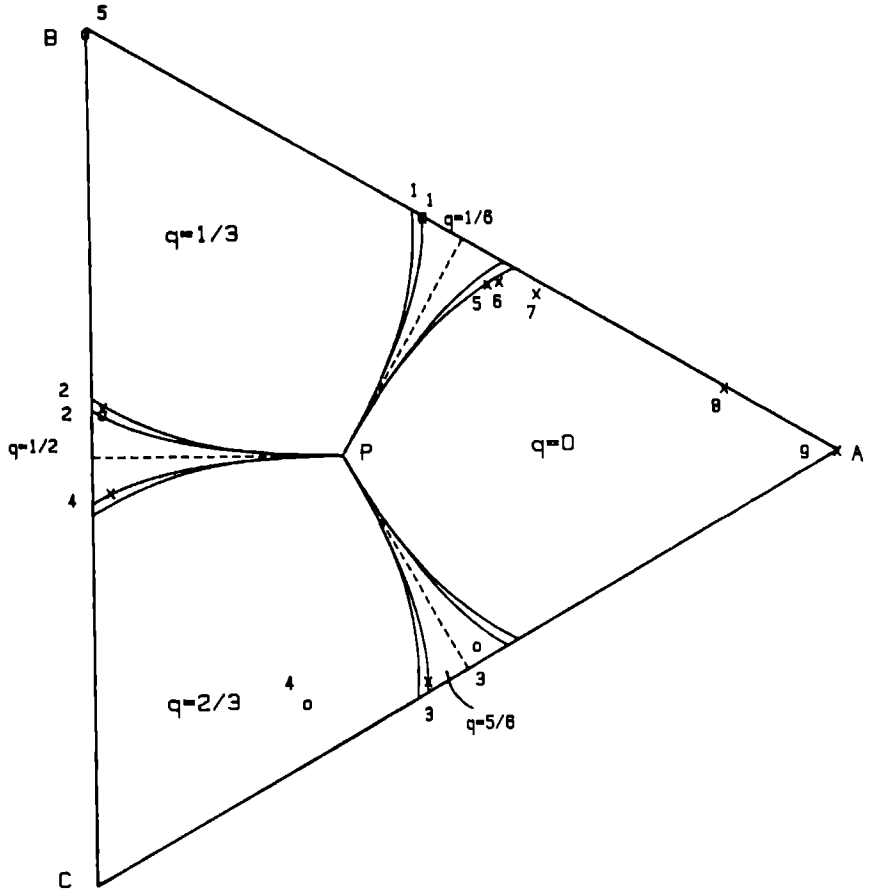

Figure 4: b

must thus, according to the procedure for finding q, described above, be the $q = 5/24$ phase. In this way, between any two phases, new phases are found. Most of them are too small to be represented in the figure. Thus the lines in the figure all consist of an infinite number of small phases.

The outer lines of the fans around $X = Y$, $Z < 1/3$ etc., are either invariant, (the lines k and o) or form fixed cycles of order two (l-n and m-j). After many transformations, they all map onto the para-point P. These lines have pre-images in the fans, being the various separation lines between the phases. In Fig. 4a, the pre-image l^{-1} is the left-most border of the line shown in the figure. l^{-2} is also indicated. All these lines are associated with the attractive eigenvalue of P. In Fig. 4b, the real phase diagram is drawn for $d = 4$, $\lambda = 0.6$. In this case, the $(2m + 1)/24$ phases are too small to be resolved. The complicated structure of the lines separating the phases comes out clearly if we take two starting points lying both on the line separating the $q = 1/6$ from the $q = 1/4$ region, but that are in fact on different positions. If we follow the images of these points, marked with 'o' and 'x' resp., we see that they end up in different points. The point 'o' is mapped after 3 iterations onto the $q = 2/3$ region, which will end up in the fixed cycle BC, and one can verify that the starting point lies in the 5/24 phase. Similarly, the 'x'-starting point lies in the 3/16 phase and ends up in A.

One can see that there are $q = m/3 \cdot 2^n$ phases for every value of n by noting that it is therefore necessary that after n transformations (n arbitrary) there must be points that map for the first time onto the regions $q = 0$, $1/3$ or $2/3$. The pre-images of these last regions are wedges extending from the para-point P to one of the edges of the triangle. As these edges are mapped *in* the triangle, the wedges have again wedges in the fans as their pre-image. After n steps going back, one thus finds the wedges corresponding to the $m/2^n \cdot 3$ phases.

So if we move across the fan at $X = Y$, $Z < 1/3$ parallel to the edge of the triangle, we find an infinite number of q values rising monotomically from 0 through values $m/2^n \cdot 3$ to $1/3$. The graph of q vs. X has an incomplete devil's staircase structure, with self-similarity [1] (Fig. 5). In Fig. 6, the phase diagram in the $kT/J - X$ plane is given for $Z = 10^{-4}$.

This diagram should be compared with phase diagrams as those found by Yeomans and Fisher [16] and Huse [11] for the chiral clock model, and

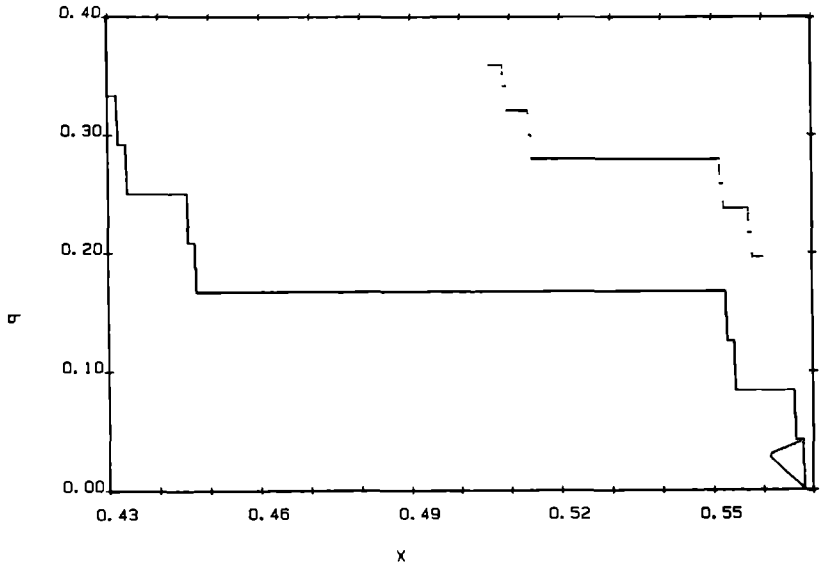

Figure 5: Behaviour of the wave vector q vs. X at $d = 4$, $w = 0.6$. z is kept fixed at 10^{-8}. The staircase shown upper right is an enlargement of the almost vertical step indicated at the right bottom of the graph.

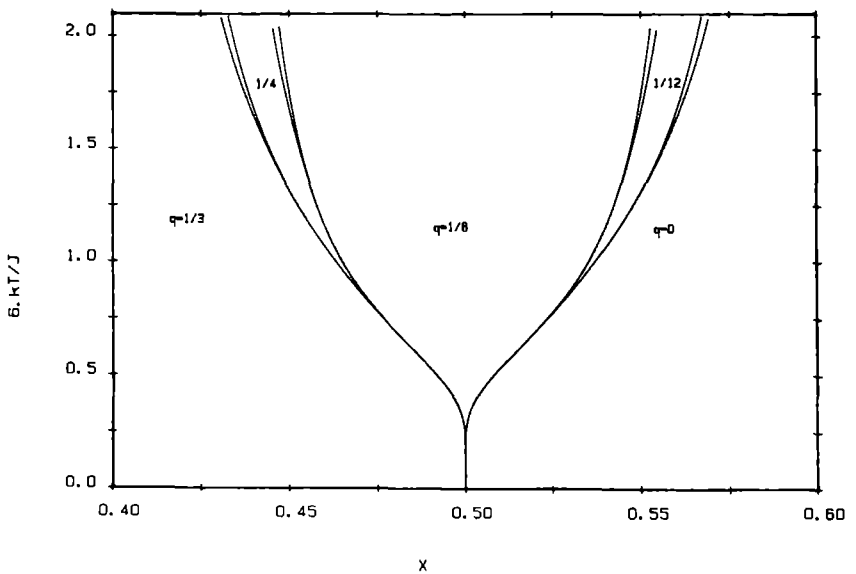

Figure 6: Phase diagram in the $kT/J - X$ plane. Z is kept constant at 10^{-4}. $d = 4$, $w = 0.6$. The separation lines shown consist of an infinite number of narrow phases.

by Fisher and Selke [19, 20] and Bak and von Boehm [21] for the ANNNI model. One should note that the separation lines represented, comprise all an infinite number of phases.

The phase diagram resembles the one obtained by Huse (for $d \geq 2.125$) in the values taken by the modulation vectors but the unphysical aspect of slivers of paramagnetic phase extending to $T = 0$ in between the modulated phases is absent. However, a comparison with the phase diagram of Yeomans and Fisher shows that there is only a superficial match between the two. A persistent point of discrepancy are the values of q taken by the higher order modulated phases, which, according to Yeomans and Fisher should be $q = m/3(2n+1)$ and $m/3(2n+3)$. As these latter values have only a single accumulation point, this also accounts for an essential difference in the devil's staircase structure ("incomplete" devil's staircase in the present case vs. "devil's top step" in the low temperature expansion). As already noted by Huse, this discrepancy must probably be attributed to the a priori choice of fixed rescaling length in the renormalization procedure.

Any other choice of l will naturally lead to the same problems, or give even worse results, as in the case $l = 3$, where there are around the lines $X = Y$, $Z < 1/3$ etc. regions of paramagnetic phase, extending from P to the edge of the triangle. If we choose $l = 1 + \epsilon$ as a renormalization constant, we cannot identify the various q-values of the phases as in the simple $l = 2$ case. According to Yeomans and Fisher, the mechanism leading to the second order phases $m/9$, is spin flips at corresponding sites in neighbouring layers. As can be seen from the deviation of the renormalization equations, this mechanism will not alter Eq. (2.6), so that we will not find these new phases. They are, however, found with $l = 3$ but in that case the important $q = 1/6$, $1/2$ and $5/6$ are represented as paramagnetic phases as noted above.

It turns out that the non-analytic structure of the renormalization transformation Eq. (2.6), which yields the correct first order transition in first order in w, is responsible for further unphysical transition lines within the modulated phases.

Consider for example, the $q = 0$ phase. As we have seen in the beginning of this section, the free energy is given by

$$f(X, Y, Z) = \lim_{n \to \infty} l^{-nd} \ln \tilde{X}_n \tag{3.15}$$

in this region.

If two starting points lie on both sides of the line $Y^2 = XZ$, $X > 1/3$, $d\tilde{Z}_1/dX$ for both points differs in order w.

Because

$$\tilde{X}_2 = \tilde{X}_1^{2p}(1 + 4w\frac{\tilde{Y}_1\tilde{Z}_1}{\tilde{X}_1}), \ldots \tag{3.16}$$

there will be a jump in the first derivative of f of second order in w.

The same argument holds for any two points that come to lie on both sides of $Y^2 = XZ$ after an arbitrary number of renormalization steps, which yield jumps of order higher than two in w, in the derivative of f.

In view of the results discussed above one must conclude that attempts to arrive at a more accurate description of modulated phases at low temperatures via a Migdal Kadanoff renormalization procedure along the lines of Ref. [11], although possible in low order, appear to fail in higher order.

Acknowledgements

We thank Dr. T. Janssen for reading the manuscript and useful discussions.

This work is part of the research program of the Stichting voor Fundamenteel Onderzoek der Materie (Foundation of Fundamental research of Matter) and was made possible by financial support from the Nederlandse Organisatie voor Zuiver Wetenschappelijk Onderzoek (Netherlands Foundation for the Advancement of Pure Research).

References

[1] P. Bak, Rep. Prog. Phys. **45** , 587 (1982).

[2] W. Selke, Modulated structures in a simple Ising model, in: *Modulated Structure Materials, T. Tsakalakos, ed.* (Nijhoff, Dordrecht 1984) p. 23.

[3] J.M. Yeomans, in: *Solid State Physics, vol. 41*, H. Ehrenreich, F. Seitz and D. Turnbull, eds (1987).

[4] R.J. Elliot, Phys. Rev. **124** , 346 (1961).

[5] S. Ostlund, Phys. Rev. B**24** , 398 (1981).

[6] K.G. Wilson and J. Kogut, Phys. Reports **12** C, 75 (1974).

[7] S.K. Ma, Rev. Mod. Phys. **45** , 589 (1973).

[8] Th. Niemijer and J.M.J. van Leeuwen, *Renormalization theory and critical phenomena in Phase transitions and critical phenomena, C. Domb and M.S. Green (eds.)* (Academic Press, New York 1976).

[9] S.R. McKay, A.N. Berker and S. Kirkpatrick, J. Appl. Phys. **53** , 7974 (1982).

[10] S.R. McKay, A.N. Berker and S. Kirkpatrick, Phys. Rev. Lett. **48** , 767 (1982).

[11] D.A. Huse, Phys. Rev. B**24** , 5180 (1981).

[12] A.A. Migdal, Zh. Ekzp. Teor. Fiz. **69** , 1457 (1975).

[13] L.P. Kadanoff, Ann. Phys. **100** , 359 (1976).

[14] J.M. Yeomans and M.E. Fisher, J. Phys. C **14** , L835 (1981).

[15] J.M. Yeomans, J. Phys. C **15** , 7305 (1982).

[16] J.M. Yeomans and M.E. Fisher, Physica **127A** , 1 (1984).

[17] R. Lipowski and H. Wagner, Z. Phys. B**42** , 355 (1981).

[18] B. Nienhuis and M. Nauenberg, Phys. Rev. L **35** , 477 (1975).

[19] M.E. Fisher and W. Selke, Phys. Rev. Lett. **44** ,1502 (1980).

[20] M.E. Fisher and W. Selke, Phil. Trans. R. Soc. **302** , 1 (1981).

[21] P. Bak and J. von Boehm, Phys. Rev. B **21** , 5297 (1980).

Chapter 3

Analysis of a new set of renormalization equations for the Kosterlitz-Thouless transition

A new and more direct derivation is given of an extended set of renormalization equations for the two dimensional Coulomb gas. Our equations are equivalent to those proposed by Minnhagen, but are cast in the form of ordinary renormalization equations. It turns out that the difference with the usual renormalization equations is due to the fact that the boundary conditions to be used are of a mixed type: two of them appear as initial conditions, the remaining ones as conditions at the end of a trajectory. The striking new features found by Minnhagen, such as the nonuniversal jump in the inverse dielectric constant and the presence of a first order transition at higher densities, are a direct result of the possibility (due to the mixed boundary conditions) of having crossing trajectories. These crossing trajectories were also found by Minnhagen *et al.*, but only in the high temperature region as multiple solutions of their integral equations. Finally we show that the rather ad hoc criterion adopted by Minnhagen *et al.* for selecting the equilibrium solution, indeed corresponds to the one with the smaller free energy, at least in the cases considered by these authors.

Published in Phys. Rev B **38**, 147-163 (1988)

3.1 Introduction

The Coulomb gas (CG), which is a two-dimensional plasma of interacting charges, plays a central role in the study of 2D critical phenomena. It has been shown [1], that many 2D systems that exhibit critical behaviour, can, at or near the critical point, be connected to the Coulomb gas.

The phase diagram of the CG has been analysed in the Kosterlitz-Thouless [2] (KT) renormalization group (RG) theory, which predicts for low charge densities a continuous transition, associated with an unbinding mechanism of dipole pairs. This transition is characterized by a jump of the renormalized coupling constant $\tilde{K}$ (or inverse dielectric constant) from a universal value to zero. This universal value is connected to critical exponents in e.g. the XY model. The high temperature [Debye-Hückel (DH)] region, where the screening of the Coulomb interaction is strong, was considered by Young and Bohr [3].

Recently, Minnhagen *et al.* [4] have derived a rather intriguing set of integral-differential equations for the renormalized coupling constant $K(l)$ and fugacity $z(l)$ using a different approach than Kosterlitz. His equations reduce to the KT renormalization equations for low values of the fugacity z.

However, when the fugacity exceeds a certain treshhold z_c, the KT transition is followed, after a further increase of temperature by a first-order transition. Moreover, at still higher fugacities (exceeding a second treshold value z_c^*), only the first order transition remains, now with a nonuniversal jump in $\tilde{K}$. An important property of the equations is that they also yield the right behaviour for the renormalized effective potential in the DH region, a feature not present in KT theory.

We have derived, using the same starting points as Minnhagen, a set of equations equivalent to the ones he found, but which have the following advantages: (i) they are simple to derive and (ii) they have the form of autonomous differential equations, i.e. appear like ordinary RG type equations. In the context of our equations, it will turn out that the new features of the Minnhagen theory (in particular the nonuniversal jump in $\tilde{K}$) are a result of the fact that the boundary conditions, specifying a certain RG trajectory, turn out to be of a mixed type: two of them are initial conditions but the remaining ones are conditions on the trajectory for $l \to \infty$.

3.2 Analysis of the renormalization equations

Derivation

We start from the following Hamiltonian:

$$-\beta\mathcal{H}_{CG} = -K\sum_{\mathbf{r}_i,\mathbf{r}_j} m(\mathbf{r}_i)m(\mathbf{r}_j)V(\mathbf{r}_i-\mathbf{r}_j) + \ln z\sum_{\mathbf{r}_i} m^2(\mathbf{r}_i). \qquad (1)$$

$m(\mathbf{r}_i)$ is the charge located at $\mathbf{r}_i$, it can take only the values 1 and -1; $K = 1/T$. The plasma is neutral, i.e. $\sum_{\mathbf{r}_i} m(\mathbf{r}_i) = 0$ The charges have a minimum separation a. $V(r)$ is the Coulomb potential: $V(r) = \ln(r/a)$.

In the derivation that follows, the "linearly screened potential" $V_L(r)$ plays a crucial role: it is the effective interaction felt by two infinitesimal charges with mutual distance r that are added to the integer charge system. To be more specific, let $Z(\alpha, r)$ be the partition function of the system with the two charges α and $-\alpha$ present at a distance r. Then in a cumulant expansion, we write:

$$\ln Z(\alpha, r) - \ln Z_{CG} = \frac{1}{2}\alpha^2\frac{\partial^2}{\partial\alpha^2}\ln Z(\alpha, r)|_{\alpha=0} + \dots \qquad (2)$$

$V_L(r)$ is defined as the part of the free energy difference proportional to α^2:

$$V_L(r) \equiv \frac{T}{2}\frac{\partial^2}{\partial\alpha^2}\ln Z(\alpha, r)|_{\alpha=0}. \qquad (3)$$

This leads then in a straightforward way to the well known linear screening formula:

$$\hat{V}_L(k) = \frac{2\pi}{k^2}\left[1 - \frac{2\pi}{k^2}\hat{g}(k)\right] \qquad (4)$$

where $\hat{V}_L$ and $\hat{g}$ denote the Fourier transforms of $V_L(r)$ and $g(r)$ respectively.

The correlation function of the Coulomb gas for pairs of opposite charges is given by

$$g_{\pm}(r) = -2z^2\frac{Z(1, r)}{Z_{CG}} \approx -2z^2 e^{V_L(r)/T} \qquad (5)$$

In the approximation on the right hand side, we have neglected higher order cumulant terms (of order α^4) that are present in Eq. (2). As the dominant

contribution to the higher order cumulant terms comes from clusters of four charges forming a quadrupole, it generates corrections of order a^2/r^2. This in contrast to the first order cumulant term which involves dipoles, yielding a contribution of order $\ln(r/a)$ (compare e.g. the Kosterlitz renormalization procedure).

The total correlation function now reads, in this approximation:

$$g(r) \approx -2z^2(e^{V_L(r)/T} - e^{2V_L(\infty)/T}e^{-V_L(r)/T}) \tag{6}$$

where the second term represents the contribution of equal charge pairs, $2V_L(\infty)$ is the creation energy for such a pair at zero distance. For a derivation of this formula from a cumulant expansion in the sine-Gordon model, see Minnhagen, Ref. 4.

Equations (4) and (6) both give a relation between $V_L(r)$ and $g(r)$. The basic observation of Minnhagen is that the renormalization group equations can be seen as a set of equations that determine a self consistent solution to (4) and (6). In this respect his approach is most close to the derivations given by José *et al.* and Young [3] of the KT renormalization equations. The difference is that (as we shall see in more detail below) José *et al.* and Young determine a selfconsistent solution for the leading logarithmic part of the potential only, while Minnhagen finds a full solution. Of course, Minnhagen's equations are not completely consistent, as higher order contributions to the effective potential are also generated by the higher order cumulant terms that were neglected. Nevertheless, a strong point in favor of his equations is that the correct description is found of both the low temperature KT phase and the high temperature DH phase.

As Eq. (4) is formulated in k-space, we first transform it to real space, and get:

$$g(r) = \frac{T}{2\pi}\Delta\left[\delta(r) - \frac{T}{2\pi}\Delta V_L(r)\right] \tag{7}$$

Realizing that $\Delta = \frac{1}{r}\frac{d}{dr}(r\frac{d}{dr})$ and setting $l = \ln(r/a)$, we find

$$g(r) = \frac{-T}{4\pi^2}\frac{1}{r^4}\left[V_L''''(l) - 4V_L'''(l) + 4V_L''(l)\right], \quad l > 0. \tag{8}$$

where the primes denote derivatives with respect to l.

We define

$$K(l) = \frac{-1}{4T}\left[V_L'''(l) - 4V_L''(l) + 4V_L'(l)\right]. \tag{9}$$

So

$$\frac{dK}{dl} = \frac{\pi^2 r^4}{T^2} g(r). \tag{10}$$

Reinserting Eq. (9) in Eq. (7) and integrating, using the fact that $V_L(r) = 0$ for $r < 1$, one finds from the δ-function appearing in (7) the initial condition $K(0) = 1/T$. We interpret $K(l)$ as a scaled (renormalized) coupling constant.

Combining finally Eq. (8), (10) and (6), we have:

$$\begin{aligned} \frac{dK}{dl} &= \frac{-1}{4T}\left[V_L''''(l) - 4V_L'''(l) + 4V_L''(l)\right] \\ &= -\frac{2\pi^2 z^2 r^4}{T^2}\left[e^{V_L(r)/T} - e^{2V_L(\infty)/T} e^{-V_L(r)/T}\right] \end{aligned} \tag{11}$$

This equation for $V_L(r)$ now has to be solved for fixed parameters z and T.

We will first examine how this equation compares with the KT and DH theory.

Comparison with KT and DH theories

Observe that the screened potential $V_L(r)$ should not grow stronger than the unscreened potential $-\ln(r/a)$. Two possibilities then remain: (i) $V_L(r)$ still grows logarithmically (with a smaller coupling constant) in which case $V_L(r) \to -\infty$ as $r \to \infty$, (ii) $V_L(\infty)$ is finite. In case (i), $V_L(\infty) \to -\infty$, so we get

$$g(r) = -2z^2 e^{V_L(r)/T} \tag{12a}$$

and

$$\frac{dK}{dl} = -\frac{2\pi^2}{T^2} z^2 e^{4l} e^{V_L(r)/T} \equiv -\frac{2\pi^2}{T^2} z^2(l) \tag{12b}$$

where we have defined

$$z(l) = z e^{2l + V_L(r)/2T}. \tag{13a}$$

If we furthermore define

$$f(l) = \frac{-1}{T}\frac{dV_L(l)}{dl} \tag{13b}$$

and $\tilde{z} = (2\pi^2/T^2)z^2(l)$, we find, using Eqs. (9) and (12):

$$\frac{dK}{dl} = -\tilde{z}(l) \tag{14a}$$

$$\frac{d\tilde{z}}{dl} = \tilde{z}(l)\,[4 - f(l)] \tag{14b}$$

$$\frac{df}{dl} = q(l) \tag{14c}$$

$$\frac{dq}{dl} = 4\,[q(l) - f(l) + K(l)] \tag{14d}$$

These equations have the appearance of RG equations in a four dimensional parameter space.

The first two equations are the same as those obtained by Minnhagen by a more elaborate procedure, if we set

$$f(l) = \int_0^\infty dx e^{-x} K(l + x/2).$$

Differentiating this integral twice leads to Eqs. (14 c) and (14 d). The KT renormalization equations are retrieved if one neglects terms of order $a/r(= e^{-l})$ and higher in $V_L(r)$. Then $V_L(r) = -TKl$, and from Eqs.(9) and (13b) it follows that $K(l) \equiv f(l)$, hence:

$$\frac{dK}{dl} = -\tilde{z}(l) \tag{15a}$$

and

$$\frac{d\tilde{z}}{dl} = \tilde{z}(l)\,[4 - K(l)]\,. \tag{15b}$$

We conclude that the KT theory should in fact not be seen as a truncated expansion in the fugacity z, but rather as a truncation in the expansion of the screened potential in powers of (a/r). This point has also been stressed by Nienhuis [1] in a careful analysis of the Kosterlitz renormalization procedure. Of course the two expansions are related as the neglect of powers of a/r in the potential is better justified for a low density plasma where the charges are on the average farther apart.

The second possibility, $V_L(r)$ finite, leads to the Debye Hückel behavior. In this case,

$$g(r) = -2z^2 e^{V_L(\infty)/T} \left(e^{[V_L(r) - V_L(\infty)]/T} - e^{-[V_L(r) - V_L(\infty)]/T}\right). \tag{16}$$

Anticipating an exponential decaying solution for the screened potential: $\tilde{V} \equiv V_L(r) - V_L(\infty) \approx e^{-r/\xi}$, one may rewrite equation (11) as a differential equation in r. Keeping only the first two terms in a ξ/r expansion yields:

$$\left[\frac{d^4}{dr^4} + \frac{2}{r}\frac{d^3}{dr^3}\right] \tilde{V}_L(r) = \xi^{-4}\tilde{V}_L(r) \tag{17}$$

with the Debye screening length defined by

$$\xi^{-2} = \frac{4\pi z}{T} e^{V_L(\infty)/2T}. \tag{18}$$

The solution of this equation (to leading order in ξ/r) is indeed the familiar Debye Hückel screening potential:

$$\tilde{V}_L(r) = C\frac{e^{-r/x_1}}{\sqrt{r/\xi}} \tag{19}$$

full solutions of the RG equations

We now turn to the full solution of Eq (11). First we discuss the critical (KT) region, where $V_L(r) = -\infty$, so Eq. (11) reduces to Eq. (14). In this region, we have four variables K, $\tilde{z}$, f and q that appear in Eq. (14), but there are only two initial conditions, namely $K(l = 0) = 1/T$ and $\tilde{z}(l = 0) = (2\pi^2/T^2)z^2$. The other two come from the restriction that $V_L(r)$ should not diverge faster than logarithmic for large r. To see how this leads to two more conditions, note that from Eq. (14), there exists a fixed line given by $\tilde{z} = q = 0$; $f = k$. This is the Kosterlitz-Thouless vacuum fixed line. The fixed line is repulsive in all directions for $K < 4$ and it is attractive in one direction for $K > 4$ (the value 4 is the universal number occurring in KT theory). Thus there is a plane in the four dimensional parameter space that is attracted to the part of the fixed line where $K > 4$. If one considers a runaway solution that does not start this plane, then for this solution, $V_L(r)$ diverges as r^2 for large r. Thus there are two extra conditions, resulting from the demand that the starting point should lie in this plane. We calculated the shape of the plane attracted by this fixed line numerically from Eq. (14).

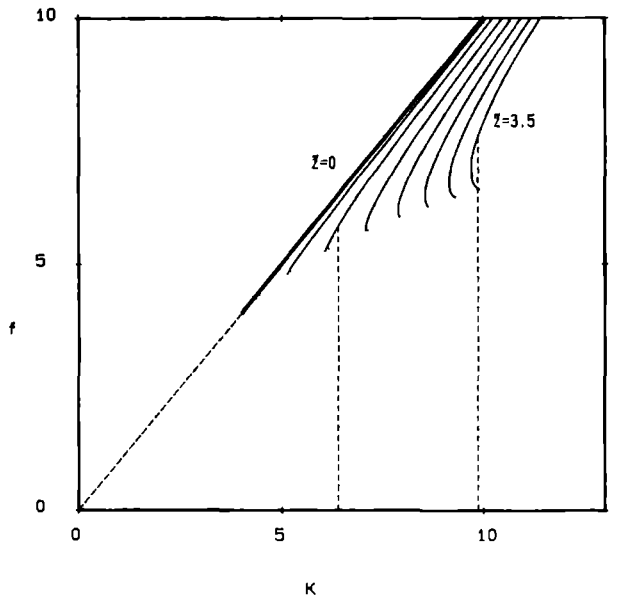

Figure 1: Contour lines of constant $\tilde{z}$ in the $f - K$ plane of the attraction domain of the KT fixed line (heavy drawn). For a given initial value of K and $\tilde{z}$ (or, equivalently, K and z), the corresponding initial value of f is obtained by an intersection of these contours with a vertical line.

In Fig. 1 the form of this plane is represented by a plot of the contour lines for fixed $\tilde{z}$ values in the $f - K$ plane.

The starting value $f(0)$ of a curve with initial conditions $K(0)$ and $\tilde{z}(0)$ is found by intersecting the line with constant $K(0)$ with the contour for $\tilde{z}(0)$ as shown in Fig. 1. The starting value for q is found by a similar procedure. From Fig. 1 it is seen that the intersections become multivalued for $\tilde{z} > \tilde{z}_c \approx 2.8$, $K > 6.99$. The choice for which of these curves yields the correct solution is dictated by the condition that it should posses the smallest free energy.

In fact, some thermodynamics shows that

$$F = -T\left[\ln Z(\beta = 0) - \int_0^\beta < E(\beta) >\right] \tag{20}$$

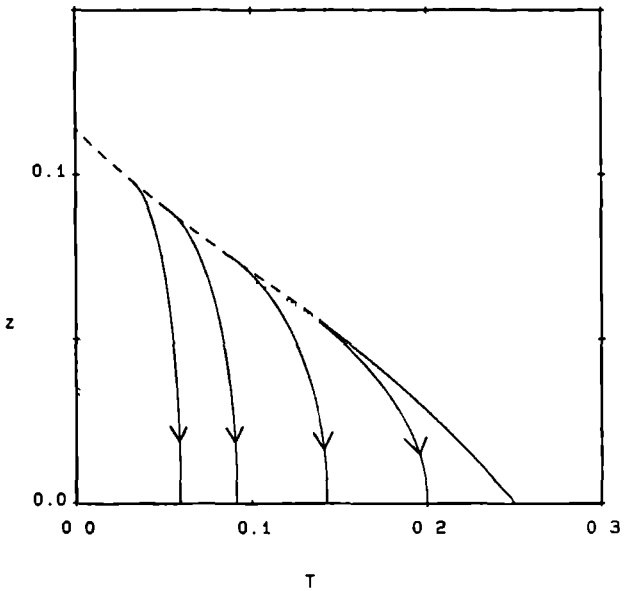

Figure 2: Phase diagram of the critical region. Curves marked with arrows are stable RG trajectories. The drawn line starting from $(T, z) = (0.25, 0)$ and the dotted line, form together the trajectory that is attracted by $K = f = 4$, $z = 0$ (see Fig. 1).

where $\beta = 1/kT$ and

$$\frac{E}{N} = TK \sum_{\mathbf{r}} g(\mathbf{r}) V(\mathbf{r}). \tag{21}$$

Here $V(r)$ is the original, unscreened potential and $g(r)$ can directly be obtained from $\tilde{z}(l)$ by virtue of Eq. (13a).

In applying this free energy condition for the solutions, one can show that the solution with the largest starting value $f(0)$, i.e. the solution corresponding to the upper intersection point in Fig. 1 is the stable one.

This results in the phase diagram of Fig. 2. The part $\tilde{z} < \tilde{z}_c^*$ of the dotted borderline in Fig. 1, is the is the drawn line in Fig. 2, marking the phase boundary for low z. The part $\tilde{z} > \tilde{z}_c^*$ of this line continues in the phase diagram as a dotted line above which multiple solutions exist. Points at this dotted line still have a trajectory which is attracted by the point $f = K = 4$, $\tilde{z} = 0$, but these trajectories now represent the metastable phase. The dashed line in the phase diagram represents the boundary of the

critical phase for $\tilde{z} > \tilde{z}_c^*$, it corresponds in Fig. 1 to the points where the contours have vertical slopes. Trajectories starting at these points reach the fixed line at $K > 4$ ($T < 1/4$ in Fig. 2). As we will see below, beyond the phase boundary (in the DH region), the coupling constant K renormalizes to zero. So across the dashed phase boundary in Fig. 2 there is a jump in the renormalized coupling constant $\tilde{K}$ larger than the universal value 4.

The argument which is usually given for the universal jump is based on the observation that a phase boundary (i.e. separatrix) should correspond to a trajectory in this case, the trajectory terminating at the point $\tilde{z} = 0$, $K = f = 4$. As the KT equations are correct as $z \to 0$, the value of $\tilde{K} = 4$ should be universal and independent of the extension of the theory with higher order terms. We now see that this argument fails due to the unusual boundary conditions that have to be adopted.

Outside the critical region, we have Eq. (11) with $V_L(\infty)$ finite, which leads to [see Eq. (16)], with $\tilde{V}_L(r) = V_L(r) - V_L(\infty)$:

$$\frac{1}{T}\left[\tilde{V}_L''''(l) - 4\tilde{V}_L'''(l) + 4\tilde{V}_L''(l)\right] = \frac{r^4}{2\xi^4}\left[e^{\tilde{V}_L(l)/T} - e^{-\tilde{V}_L(l)/T}\right] \tag{22}$$

with $\tilde{V}_L(l) \to 0$ for $l \to \infty$.

One has now

$$\tilde{z}(l) = \frac{1}{8}\frac{r^4}{\xi^4} e^{\tilde{V}_L(l)'T}. \tag{23a}$$

If one defines

$$\tilde{w}(l) = \frac{1}{8}\frac{r^4}{\xi^4} e^{-\tilde{V}_L(l)/T}. \tag{23b}$$

it is possible to cast Eq. (20) in the form of renormalization equations, just as we did in Eq. (14):

$$\frac{dK}{dl} = -\tilde{z}(l) + \tilde{w}(l), \tag{24a}$$

$$\frac{d\tilde{z}}{dl} = \tilde{z}(l)\,[4 - f(l)] \tag{24b}$$

$$\frac{d\tilde{w}}{dl} = \tilde{w}(l)\,[4 + f(l)] \tag{24c}$$

$$\frac{df}{dl} = q(l) \tag{24d}$$

$$\frac{dq}{dl} = 4\,[q(l) - f(l) + K(l)] \tag{24e}$$

The boundary conditions are

$$K(0) = \frac{1}{T} \ , \tag{25a}$$

$$\tilde{z}(0) = \frac{2\pi^2}{T^2 z^2 a^4 e^{V_L(\infty)/T} = \frac{2\pi^2}{T^2} z^2 a^4} e^{-V_L(0)/T} \tag{25b}$$

and

$$V_L(r) \rightarrow 0 \ \text{as} \ \ r \rightarrow \infty \tag{25c}$$

We used Eq. (22) [or equivalently Eqs. (24)] with the boundary conditions Eqs. (25) to get the solutions, some of which are represented in the $T-z$ diagram of Fig. 3. These solutions form a plane in the five-dimensional (5D) parameter space of Eqs. (24). The contours of constant $\tilde{z}$ of this plane are represented, together with those of Fig. 1, in Fig. 4. The contours join smoothly at the trajectory attracted by $K = f = 4$, $\tilde{z} = 0$ (the dotted line). One can see from Fig. 3 that the DH region overlaps with the KT region. However, from numerical inspection of the free energy of the solutions, using Eq. (20) and (21), one concludes that the KT solutions are the stable ones here. Outside the KT region, for $z_c < z < z_c^*$ with $\tilde{z}_c \approx 0.45$, close to the phase boundary, still multiple DH solutions are found. Selecting the one with the lowest free energy generates a first-order transition within the DH region (see Fig. 5 which is an enlargement of Fig. 4). This line is in fact the continuation of the phase boundary of the KT region represented as the dashed line in Fig. 3. The entire transition line is first order: neighbouring points on both sides of this line correspond to initial points with a finite separation in the 5D parameter space of Eq. (24). So the trajectories do not lie close together, and there is a latent heat associated with the transition. Moreover, the charge density, which is given by

$$n = \int_{|\mathbf{r}|>a} g(\mathbf{r}) d^2 r \tag{26}$$

because of charge neutrality, has a jump across this line. At $z = z_c^*$ the density becomes approximately twice as large at the transition.

The first order transition is again a result of the fact that the boundary conditions in our case are different from those in ordinary RG theory. Of course, in the four or five dimensional parameter space of Eqs. (14) and (24)

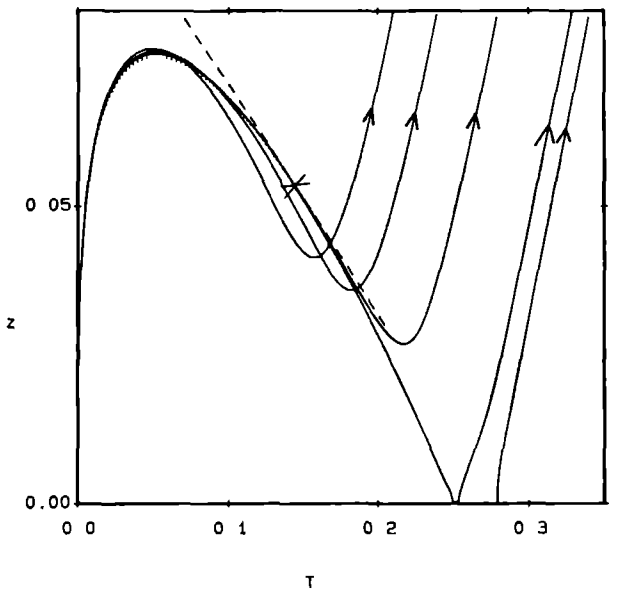

Figure 3: Phase diagram. Curves marked with arrows are Debye-Hückel trajectories. The dashed first order phase boundary continues to a first order transition line *in* the DH region.

respectively, a unique trajectory is passing through every point. The fact that these trajectories should have the correct asymptotic behavior and be projected onto the two-dimensional (T, z) space, causes the non-uniqueness in this latter space.

3.3 Conclusions

Apart from its simplicity, which we feel brings out the relation with the usual RG theory more clearly, our analysis adds two extra features to the approach of Minnhagen. First, we find two solutions in a part of the critical region, for given $K(0)$ and $z(0)$, whereas Minnhagen obtained only one, by a self consistent iteration procedure (in fact, the extra solution we found, is a fixed, but unstable trajectory under his procedure). Secondly, we feel that our free energy criterion for the selection of the correct solution whenever there is more than one possibility, is more fundamental than the rather *ad*

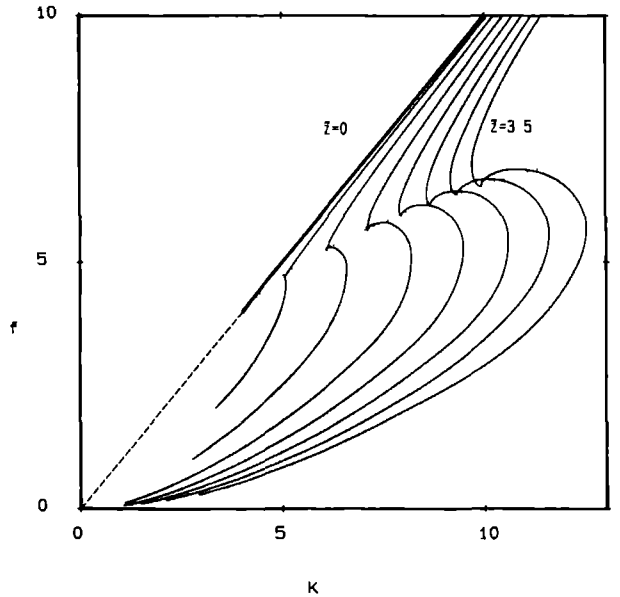

Figure 4: Contour lines of constant $\tilde{z}$ in the $f - K$ plane for KT, resp DH trajectories.

hoc choice of Minnhagen for the solution with the longest screening length. If one extends this choice for the KT region by selecting the solution with the slowest decay, one obtains in fact the second solution that Minnhagen did not find by his method. One would arrive then at a rather peculiar phase diagram. In the DH region, our criterion gives the same results as Miñnhagen's, so our final phase diagram does not differ from his.

As far as the validity of this phase diagram is concerned, numerical simulations by Caillol and Leveque [6] indicate that indeed the second-order transition for low charge densities becomes first order at higher densities. Saito [7] has found first order transitions for a modified Coulomb gas, modelling 2D crystal surface melting [8]. However, in this case it appears that this transition is driven by "grain boundaries" that are a consequence of the vector character of the charges, a feature which is not present in the ordinary Coulomb gas.

Minnhagen [9] proposed the fully frustrated XY model [10] as an example of a system to which his theory should apply. This model can be mapped onto an Ising model in which fractional charges 1/4 and $-1/4$, in-

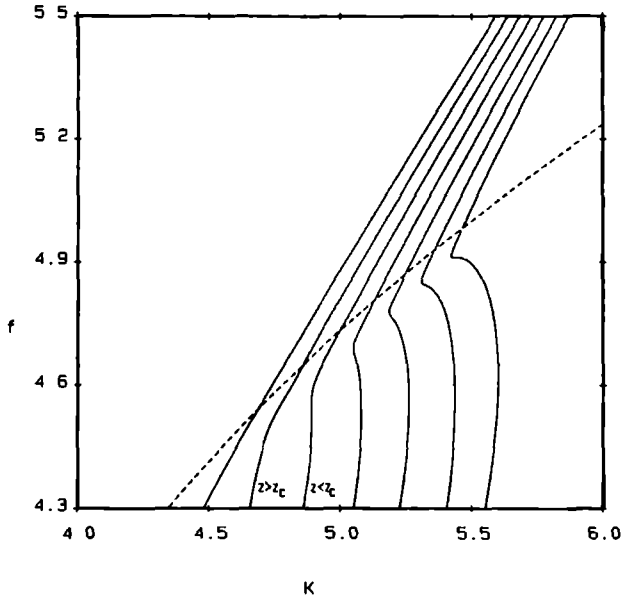

Figure 5: enlarged detail of Fig. 4.

teracting through the Coulomb potential, are present at the corners of the Ising domain walls. Nonuniversal jumps in the inverse dielectric constant have indeed been found in this model. In a previous paper [10], we have proposed a different explanation of this nonuniversality: we suggested that the Ising transition triggered the KT transition through the proliferation of free fractional charges, which would also result in a nonuniversal jump, but in this case the transition would be second order. Further analysis of our simulation data give no indication for a first-order transition, which makes it rather doubtful that the Minnhagen scenario is responsible for the nonuniversality found.

To check the validity of Minnhagen's theory further, one should therefore perform more extensive Monte Carlo calculations on the integer charge

Coulomb gas.

Acknowledgements

We thank O. Abu-Zeid for important discussions during the initial stages of this work.

This work is part of the research program of the Stichting voor Fundamenteel Onderzoek der Materie (Foundation of Fundamental research on Matter) and was made possible by financial support from the Nederlandse Organisatie voor Zuiver Wetenschappelijk Onderzoek (Netherlands Foundation for the Advancement of Pure Research).

References

[1] B. Nienhuis, in *Phase Transitions and Critical Phenomena* Vol. 11, edited by C. Domb and J.L. Lebowitz (Academic Press, London, 1987).

[2] J.M. Kosterlitz and D.J. Thouless, J. Phys. C **6**, 1181 (1973); J.M. Kosterlitz, J. Phys. C **7**, 1046 (1974).

[3] A.P. Young and T. Bohr, J.Phys. C **14**, 2713 (1981).

[4] P. Minnhagen, Phys. Rev. Lett. **54**, 2351 (1985), Phys. Rev. B **32**, 3088 (1985); P. Minnhagen and M. Wallin, Phys. Rev. B **36**, 5620 (1987).

[5] J.V. José, L.P. Kadanoff, S. Kirkpatrick, and D.R. Nelson, Phys. Rev. B **16**, 1217 (1977); A.P. Young, in *Ordering in Strongly Fluctuating Condensed Matter Systems. Vol B50* of *NATO Advanced Study Institute, Series B: Physics*, edited by T. Riste (Plenum, New York, 1980), p.217; J. Phys. C **11**, L435 (1978).

[6] J.M. Caillol and D. Levesque, Phys. Rev. B **33**, 499 (1986).

[7] Y. Saito, Phys. Rev. Lett. **48**, 1114 (1982), Phys. Rev. B **26**, 6239 (1982).

[8] D.R. Nelson and B.I. Halperin, Phys. Rev. B **19**, 2457 (1979).

[9] P. Minnhagen, Phys Rev B **32**, 7548 (1985).

[10] J.M. Thijssen and H.J.F. Knops, Phys. Rev. B **37**, 7738, (1988).

Chapter 4

Monte Carlo study of the Coulomb-gas representation of frustrated XY models

We construct a model consisting of a half integer Coulomb gas, corresponding to the frustrated XY model, and add an Ising interaction J to it. In this system, it is possible to vary the Coulomb interaction strength, corresponding to the vortex interaction in the frustrated model, separately from the Ising interaction of the domain walls. The model is studied theoretically and numerically to obtain the phase diagram. We observe at high J values two critical lines. One corresponds to an Ising transition, the other to a Kosterlitz Thouless transition with a jump in the helicity modulus (inverse dielectric constant) in accordance with the universal value to be expected for unit charges. At $J = 0$ the two critical branches coincide (as has been found in direct Monte Carlo simulations) to a single critical line for $J \leq 0$ which has both Ising and Kosterlitz Thouless critical characteristics. However, the jump in the helicity modulus does no longer appear to be universal further down this line.

Published in Phys. Rev. B **37**, 7738 (1988).

4.1 Introduction

In recent years, frustrated XY models have been the object of several numerical [1–7] and theoretical [6-13] studies. One reason for this interest is that arrays of Josephson junctions are believed to be modelled by such systems [14, 15]. Moreover, frustrated XY models are interesting from a theoretical point of view: as the ground state has a rotational $U(1)$ symmetry together with a $\mathbf{Z}_2$ Ising symmetry, one expects Ising as well as XY critical behavior to be possible.

The general idea, as explained for example by Korshunov and Uimin [8] (see also Halsey [13]), is that the excitations of of the model can be described by domain walls (strings), separating domains with ground states of a different helicity. At the corners of domain walls resides a net (fractional) vorticity by which these corners interact via a logarithmic potential. In a Coulomb-gas (CG) language, these corners are, in the case of a square lattice, represented by charges $q = \pm 1/4$. At high values of the domain wall energy, these charges are bound together to plaquettes of net charge $q = \pm 1$. As these plaquettes are not connected by domain walls, an ordinary Kosterlitz-Thouless (KT) transition [16, 17] is expected separating the Debye-Hückel region where these charges are free, from the region where bound dipole pairs occur. By lowering the domain wall energy one can reach a point where the domain wall free energy vanishes and the walls "melt". Depending on the value of the Coulomb coupling constant K, three scenarios are, in principle, possible. If K is so small that the charges $q = \pm 1$ are already free, an ordinary Ising transition restoring the up-down symmetry is expected. At intermediate values of K, the $q = \pm 1$ charges are bound but the $q = \pm 1/4$ charges are not bound by the Coulomb interaction. However, as the fractional charges are connected by domain walls, these charges become only free at the Ising transition point where the domain wall tension vanishes. In this case the Ising transition will be accompanied by a KT-like transition.

Finally, at still larger values of K, it is possible that the $q = \pm 1/4$ charges are still logarithmically bound when the walls melt, yielding again an ordinary Ising transition, but now to a phase which posesses still XY-like algebraic order.

Numerical work [1–4] for the frustrated XY model with a pure cosine interaction seems to indicate that the relative values of string energy and Coulomb coupling K happen to be such that the KT and the Ising transition

coincide. In order to study the full phase diagram one would like to have a model in which the domain wall energy and the Coulomb coupling can be varied independently. Several authors have proposed such models. Recently van Himbergen [5, 6] has carried out Monte Carlo simulations for frustrated XY models where the cosine interaction is altered in some other periodic function. However, it turned out that too drastic changes soon lead to a model with a completely different ground state, so that in practice only a rather limited change in the domain wall energy versus Coulomb coupling could be explored, all yielding a single transition. Berge *et al.* [7] analysed a XY model on a square lattice as a function of the ratio η between ferromagnetic and antiferromagnetic couplings in the model. However, for $\eta \neq \pm 1$, the original translational invariance of the Hamiltonian is lost so that one studies in fact a problem with a different symmetry. Moreover their method to locate the KT transition point is less convincing than the determination of a jump in the helicity modulus as is usually done [1–6,18,19].

Granato, Kosterlitz and Poulter [10] performed a renormalization group (RG) transformation on a model consisting of two coupled XY systems [11], believed to be in the same universality class as the frustrated XY models. They present a phase diagram where the KT transition coincides with the Ising transition at a point (or perhaps a short line) but as soon as the transitions are separated, the Ising transition is always into a XY ordered phase, in contrast to the scenario given above. It should be noted, however, that their paper discusses again a model with a different symmetry, which does not allow for fractional vortices that are believed to be fundamental in the transition mechanism. For the same reason, the modification of the model studied by Granato [12], cannot yield the KT transition for the fractional charges.

Perhaps the most natural way to explore the phase diagram under consideration is to start with a the Coulomb gas formulation into which the Villain form of the model can be exactly transformed [9]. An addition of an Ising interaction to the Coulomb interaction enables one to tune the Coulomb coupling and string energy separately without altering the symmetry of the model or its ground state. (In the original model this extra interaction corresponds to a four spin coupling). In this paper, we present a direct Monte Carlo analysis of this Coulomb version of the frustrated XY model. An additional advantage of this method is that it is known for the ordinary

(non-frustrated) XY model, that a Monte Carlo analysis for its Coulomb representation, where the spin wave excitations have already been integrated out, yields generally better statistics [20].

4.2 Description of the model.

The "standard form" of the frustrated XY Hamiltonian on a square lattice is given by:

$$H = K \sum_{<\mathbf{R},\mathbf{R}'>} cos(\Theta_{\mathbf{R}} - \Theta_{\mathbf{R}'} + A_{\mathbf{R},\mathbf{R}'}) \qquad (1)$$

where the sum is over nearest neighbour pairs, the $\Theta_{\mathbf{R}}$ are angle variables, and the $A_{\mathbf{R},\mathbf{R}'}$ are constants associated with the bonds subject to the constraint $\sum A_{\mathbf{R},\mathbf{R}'} = \pi$ for every plaquette.

It turns out that, apart from the symmetry that leaves the Hamiltonian invariant under a uniform rotation of all spins, two ground states are possible, with alternate chiralities (helicities) on the plaquettes, one shifted one lattice spacing as compared to the other. At finite temperatures, regions corresponding to both ground states occur simultaneously, separated from each other by domain walls. Imagine the $A_{\mathbf{R},\mathbf{R}'}$ chosen such that $A_{\mathbf{R},\mathbf{R}'} = \pi$ on alternating vertical columns and $A_{\mathbf{R},\mathbf{R}'} = 0$ everywhere else. If a vertical domain wall separates two phases with opposite chirality, the phase angle of one of these is uniquely defined with respect to the other at low temperatures [13]. If the domain wall is shifted one lattice spacing to the right, the phase difference shifts over an amount of π. So, if the domain wall has a kink that arises by shifting a part of the wall over one lattice spacing, there is a phase mismatch of π. This corresponds precisely to a vortex $1/2$ located at the kink. This fractional vortex is in fact a special case of the general rule (as explained below) that a vortex $\pm 1/4$ is located at each corner of a domain wall.

The Hamiltonians considered in Refs. 10-12 which supposedly are in the same universality class as the frustrated XY model renormalize towards a model with a $U(1) \times \mathbf{Z}_2$ symmetry described by

$$\mathcal{H} = K \sum_{\mathbf{R},\mathbf{R}'} \cos(\Theta_{\mathbf{R}} - \Theta_{\mathbf{R}'})(1 + s_{\mathbf{R}} s_{\mathbf{R}'}). \qquad (2)$$

where the $\Theta_{\mathbf{R}}$ are planar and $s_{\mathbf{R}}$ Ising spins. It is clear, however, that in this case there is no phase dependence on the location of the Ising domain

walls and hence, there are no fractional vortices associated with the corners of these walls.

The presence of these fractional vortices becomes particularly clear if one transforms the model (with an interaction of the Villain type), by integrating out the spin wave degrees of freedom, to a Coulomb gas [9]. In this Coulomb gas language, the Hamiltonian is expressed in terms of half integer charges $m_{\mathbf{r}}$ on the sites of the dual lattice corresponding to the vortices in the original model. One assumes that one can safely restrict these charges to take on the values $\pm 1/2$.

The Hamiltonian reads:

$$\mathcal{H} = K \sum_{\mathbf{r},\mathbf{r}'} m_{\mathbf{r}} m_{\mathbf{r}'} V(\mathbf{r} - \mathbf{r}') \tag{3a}$$

where the charges satisfy the neutrality condition $\sum_{\mathbf{r}} m_{\mathbf{r}} = 0$. V is the latice Green's function:

$$V(\mathbf{r}) = \frac{2\pi^2}{N^2} \sum_{\mathbf{q}} \frac{-1 + e^{i\mathbf{q}\mathbf{r}}}{4 - 2\cos q_x - 2\cos q_y} \tag{3b}$$

which, for large N and r, reduces to [17]

$$V(\mathbf{r}) \approx -\pi \ \ln r + \pi^2/2 \tag{4}$$

The ground state of the CG model is twofold degenerate and consists of an antiferromagnetic pattern of alternating $+1/2$ and $-1/2$ charges (reflecting the alternating helicities of the XY model ground state).

The energy of a straight domain wall separating the two possible ground states, can be calculated by comparing the ground state energies of a system with an even (odd) number of sites along one direction. the result is

$$E_{wall} = \frac{\pi^2}{16\sqrt{2}} K \tag{5}$$

per unit length.

In order to vary the wall energy independently, we add a nearest neighbour (antiferromagnetic) interaction to the Coulomb gas energy :

$$\mathcal{H}(J,K) \equiv 4J \sum_{<\mathbf{r},\mathbf{r}'>} m_{\mathbf{r}} m_{\mathbf{r}'} + K \sum_{\mathbf{r},\mathbf{r}'} m_{\mathbf{r}} m_{\mathbf{r}'} V(\mathbf{r} - \mathbf{r}') \tag{6}$$

In Fourier transformed variables, this extra interaction alters terms that come after the leading contribution of $(2\pi^2/q^2)K$ form the Coulomb potential. In the discrete Gaussian representation, where the inverse of this interaction appears, this leads to the presence of some further, short range interactions. Finally, a duality transformation brings the model back to the frustrated XY model where now some extra four spin interactions appear. The ground state of the model and the nature of the excitations from it remain the same, at least as long as the wall energy, which is now

$$E_{wall} = \frac{\pi^2}{16\sqrt{2}}K + 2J \tag{7}$$

remains positive.

We determined the phase diagram for the system with Hamiltonian $\mathcal{H}(J,K)$ by a Monte Carlo simulation. For convenience, periodic boundary conditions (BC) were used. It should be noticed that the cyclic boundary condition for the Coulomb gas does correspond to a more complicated BC for the frustrated XY model (the BC to be used is a cyclic one but with a phase mismatch ψ with respect to which the partition sum should be integrated).

In order to clarify the physical picture according to which only corners of domain walls carry net charges, it is useful, as noted by Halsey [13] and Korshunov and Uimin [8], to define the interaction in terms of charges $q_{\mathbf{R}}$ that are the averages of the four charges $\mathbf{r}_1, \ldots, \mathbf{r}_4$ (of the dual lattice) surrounding $\mathbf{R}$. Carrying out this idea in more detail, one finds:

$$\mathcal{H}(J,K) = -J \sum_{<\mathbf{r},\mathbf{r}'>} s_{\mathbf{r}} s_{\mathbf{r}'} + \sum_{\mathbf{r},\mathbf{r}'} \Delta V(\mathbf{r}-\mathbf{r}') s_{\mathbf{r}} s_{\mathbf{r}'} + K \sum_{\mathbf{R},\mathbf{R}'} q_{\mathbf{R}} q_{\mathbf{R}'} V(\mathbf{R}-\mathbf{R}') \tag{8}$$

where $s_{\mathbf{r}'}$ is a ferromagnetic Ising spin variable defined as $s_{\mathbf{r}} = (-1)^{x+y} 2m_{\mathbf{r}}$ and the averaged charge is given by

$$q_{\mathbf{R}} = (-1)^{x_1+y_1}(s_{\mathbf{r_1}} - s_{\mathbf{r_2}} + s_{\mathbf{r_3}} - s_{\mathbf{r_4}})/8. \tag{9}$$

The new interaction $\Delta V(\mathbf{r}-\mathbf{r}')$ that arises in this quadrupole-like expansion as a correction term is given in terms of the lattice Green's function by

$$\Delta V(\mathbf{r}) \equiv \frac{1}{4}(-1)^{x+y} K \left\{ V(\mathbf{r}) - \frac{1}{16} \sum_{i=1}^{4} \sum_{j=1}^{4} V(\mathbf{r} + \mathbf{e_i} + \mathbf{e_j}) \right\} \tag{10}$$

where the $\mathbf{e_i}$ are vectors connecting a site $\mathbf{R}$ of the dual lattice with the vectors $\mathbf{r_i}$ surrounding it. In Fourier transformed variables it reads :

$$\Delta V(\mathbf{q}) = \frac{\pi^2}{8} \frac{K(3 + \cos q_x + \cos q_y - \cos q_x \cos q_y)}{2 + \cos q_x + cosq_y} \tag{11}$$

This interaction is analytic for all q values [in contrast to the Green function $V(\mathbf{q})$] and behaves, for $\mathbf{q} \to (\pi, \pi)$ as:

$$\Delta V(\mathbf{q}) \approx \frac{\pi^2}{8} K(1 + \frac{1}{8}q^2 + \ldots) \tag{12}$$

One concludes that $\Delta V(\mathbf{r})$ is a short-range ferromagnetic Ising interaction (with decay length $\kappa = 1/4\sqrt{2}$). It can, in a first approximation be represented by a nearest neighbour Ising interaction with a coupling strength Δ chosen such that the wall energies of a long straight wall match. It is straightforward to derive from Eq. (12) that one should take $\Delta = \frac{\pi^2}{32\sqrt{2}} K$ in accordance with Eq. (5). So finally we arrive at the following (approximate) form of the Hamiltonian $\mathcal{H}(J, K)$:

$$\mathcal{H}(J, K) \approx -(J + \Delta) \sum_{<\mathbf{r},\mathbf{r}'>} s_{\mathbf{r}} s_{\mathbf{r}'} + K \sum_{\mathbf{R},\mathbf{R}'} V(\mathbf{R} - \mathbf{R}') \tag{13}$$

with $q_{\mathbf{R}}$ given by Eq. (7). The ground states are the two ferromagnetic ground states with $s_{\mathbf{r}} \equiv 1$ or $s_{\mathbf{r}'} \equiv -1$ and all $q_{\mathbf{R}} = 0$. It follows directly from the definition of $q_{\mathbf{R}}$ that a straight wall separating the two ground state configurations does not carry a charge, but that at a corner of such a wall a charge $q = \pm 1/4$ is located. The sign convention is such that following a wall from one corner to the next, opposite (equal) charges are found when the corners are separated by an even (odd) number of steps. The lowest Ising excitation, a single overturned spin, has therefore a net charge ± 1.

Before we present our numerical results for the phase diagram of the Hamiltonian Eq. (6) it is useful to collect some pieces of information based on the simplified picture Eq. (13).

4.3 Theoretical analysis of the model

It is clear, that for $K = 0$, we will have an Ising model with a transition at $J_c = 0.44$. For positive values of K, one expects the model to have still a

transition although its nature may change due to the long range nature of the Coulomb interaction. To investigate wether a cross over to a different type of transition is to be expected, we write:

$$\mathcal{H} = \mathcal{H}_{Ising} + K\mathcal{H}_{CG} \tag{14}$$

where $\mathcal{H}_{Ising}$ contains the nearest neighbour Ising interaction together with a short range Ising interaction that arises from the Coulomb Hamiltonian from terms with $|\mathbf{R} - \mathbf{R}'| \leq L$ (where L denotes an arbitrary short range cutoff). The remaining terms in the Coulomb interaction can be written in a continuum notation as:

$$\mathcal{H}_{CG} \approx \frac{\pi}{8} \int d^2 \frac{(r+r')}{2} \int_{|\mathbf{r}-\mathbf{r}'|\geq L} d^2(r-r') \frac{\partial^2 s(\mathbf{r})}{\partial x \partial y} \frac{\partial^2 s(\mathbf{r}')}{\partial x' \partial y'} \ln(|\mathbf{r}-\mathbf{r}'|) \tag{15}$$

By partial integration (absorbing boundary terms in the short range interaction) one obtains:

$$H_{CG} \approx \frac{\pi}{8} \int d^2 \frac{(r+r')}{2} \int_{|\mathbf{r}-\mathbf{r}'|\geq L} d^2(r-r') s(\mathbf{r}) s(\mathbf{r}') \frac{\partial^2}{\partial x \partial y} \frac{\partial^2}{\partial x' \partial y'} \ln(|\mathbf{r}-\mathbf{r}'|) \tag{16}$$

From Kadanoff's operator expansion [21], one knows that $s(\mathbf{r})s(\mathbf{r}')$ can be written in terms of scaling operators as :

$$s(\mathbf{r})s(\mathbf{r}') = f(\mathbf{r}-\mathbf{r}')I + g(\mathbf{r}-\mathbf{r}')\epsilon(\frac{\mathbf{r}+\mathbf{r}'}{2}) + ... \tag{17}$$

where $\epsilon(\mathbf{r})$ is the scaling operator corresponding to the Ising energy and the dots represent irrelevant scaling operators. The function $f(\mathbf{r})$ and $g(\mathbf{r})$ scale like $r^{1/4}$ and $r^{3/4}$ respectively.

Inserting this expression in (16) yields:

$$\mathcal{H}_{CG} \approx \int d^2 r \left[A \cdot I + B \cdot \epsilon(\mathbf{r}) + \ldots\right] \tag{18}$$

where A and B are finite constants as the integrals over $\mathbf{r} - \mathbf{r}'$ converge. One concludes that the only relevant scaling field that is generated by the Coulomb interaction in an expansion around the Ising fixed point, is the Ising energy operator. One expects therefore, that the transition remains Ising like, but that the transition point is shifted by an amount proportional

with K (the proportionality factor involves both the constant B and the short range Ising terms collected in H_{Ising}).

We now turn to the large J behavior. In this regime, the most important excitations are single spin flips corresponding to charge $q = \pm 1$. The system behaves now analogous to the integer charge Coulomb gas, so we expect a KT transition at $\tilde{K} = 2/\pi$, where $\tilde{K}$ is the renormalized value of K [17]. The actual transition value K_c is determined by the chemical potential μ, i.e. the formation energy for a +1 or -1 charge. This energy can be calculated from the spin model Eq. (13) or rather its exact form Eq. (8) taking into account the Coulomb interaction between the fractional charges at the corners of the plaquette. However, it is more convenient to start with the original model Eq. (6) and calculate the energy difference that results from creating a pair of charges $m_{\mathbf{r}} = \frac{1}{2}, m_{\mathbf{r}'} = -\frac{1}{2}$ to $m_{\mathbf{r}} = -\frac{1}{2}$, $m_{\mathbf{r}'} = \frac{1}{2}$. One obtains

$$\Delta E = -4K \sum_{\mathbf{r}} V(\mathbf{r}) m(\mathbf{r}) - 2KV(\mathbf{r} - \mathbf{r}') + 16J \tag{19}$$

where the first term represents the interaction with the charged background, the second term the direct Coulomb interaction and the third term the Ising energy. The first term is a constant given by

$$-2K\tilde{V}(\pi, \pi) = -\frac{1}{2}\pi^2 K,$$

and the second term can be rewritten according to Eq. (4). Collecting all constants, one finds for the chemical potential μ of a single charge:

$$\mu = 8J + \frac{1}{4}\pi^2 K \tag{20}$$

Employing the formula for K_c that results from a low fugacity expansion of the renormalization group equations [17], one finds

$$K_c = \frac{2}{\pi} + 4e^{-8J-(1/4)\pi^2 K_c} \tag{21}$$

At the transition point K_c the renormalized coupling constant $\tilde{K}$ exhibits a universal jump from the value $2/\pi$ to zero. When lowering J, formula (21) for K_c, being only valid for large μ breaks down.

The fractional charges may undergo a KT binding transition at a coupling $K_c(1/4)$ roughly 16 times larger than the KT coupling of the integer ones. However, fractional charges are always part of a domain wall (connected by strings). Two fractional charges at a distance r connected by a domain wall will have an effective interaction

$$\frac{\pi}{8} K \ln r + \alpha r \tag{22}$$

where α is the domain wall tension vanishing at the Ising transition. Hence, fractional charges will be bound whenever the system is Ising ordered. If the Ising transition takes place when $K < K_c(1/4)$, the fractional charges will become free simultaneously with the Ising transition. This means, that at that point, the charges will provide exponential screening of the Coulomb interaction, so the transition has similar features as the KT transition in that the renormalized coupling constant exhibits a jump to zero. However, it is caused here by a completely different mechanism. In this case, one would expect in particular a jump in the renormalized coupling $\tilde{K}$ that is larger than the universal KT value $2/\pi$.

4.4 Numerical Results

All the simulations were performed with Hamiltonian Eq. (6). The advantage of doing a MC simulation in the Coulomb gas [20], is that the creation of a vortex, which takes many MC steps in the XY system, is here just a matter of flipping a charge. However, the long range of the logarithmic interaction implies that in principle with every MC step many calculations are involved. In practice we start with a calculation of the Coulomb potential energy at every lattice site for some given initial configuration. This potential is then updated over the whole lattice after every succesful MC step. This procedure has the advantage that the numerical work is restricted to the relatively small number of succesful MC steps. We did not use the "enhancement factor" of Saito and Müller-Krumbhaar [20] because it is not obvious how one should implement this factor in this case.

To determine the global structure of the phase diagram, a 40×40 lattice was used, and a number of Monte Carlo steps per spin (MCS) varying from 3000 to 30000. The Ising transition is characterized by a drop in the magnetization (chirality in the XY language) and peaks in the magnetic

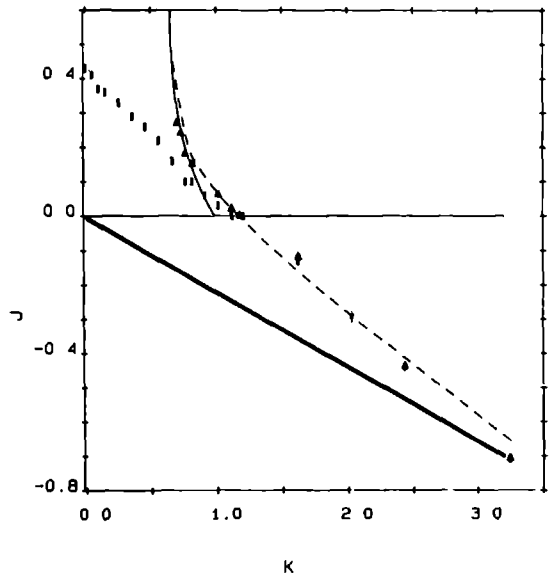

Figure 1: Phase diagram of the model Eq. (6). The triangles denote KT transition points, rectangles correspond to Ising transition points. The drawn line is the theoretical KT transition line. The dashed-dotted line is the Minnhagen prediction. The dotted line corresponds to the Ising-critical wall energy. The heavy line is the border beyond which the ground state is completely different from the ordinary frustrated XY model ground state.

susceptibility and specific heat. Based on these peaks, Ising transition points were determined and represented as rectangles in Fig. 1. The Ising line starts off as expected at the $K = 0$ axes from $J = 0.44$. The line $J = 0.44 - \pi^2 K/32\sqrt{2}$ (dotted line), is the line at which the energy of a straight domain wall is equal to the Ising critical value. The interaction between the domain wall corners causes the actual transition line to be pushed down (see Sec. 3).

The KT transition is signaled by a drop in the helicity modulus $\Upsilon = \tilde{K}/K$ where $\tilde{K}$ is the renormalized coupling constant. In the CG, this quan-

tity is the long wavelength limit of the dielectric constant [19]:

$$\Upsilon = \lim_{q\to 0} \epsilon_q^{-1} = \lim_{q\to 0} \left[1 - \frac{KV(q)}{N^2} < n(q)n(-q) > \right] \qquad (23)$$

For our calculations we took the lowest q value possible, i.e. $q = 2\pi/N$. The KT transition points are represented as triangles in Fig. 1. The low density prediction for the KT transition point, see Eq. (21), is shown in this figure as a solid line. One finds a fair agreement with the numerical data for high values of J as expected. Recently Minnhagen [22-24] proposed an alternative set of renormalization equations for $\tilde{K}$, which attempt to take some of the further terms in the fugacity expansion into account by a more careful treatment of the short range terms generated in the potential. Indeed his equations reduce to the usual ones for low densities. For higher densities he finds quite different results. First, as to be expected, the transition line that follows from his equations deviates from the low density formula given above [Eq. (21)] (in fact, Minnhagen's transition line is rather close to that of Amit *et al.* [25] who treated the next term in the density expansion exactly). We calculated the transition line, using Minnhagen's equations, for the present case. The result is shown in Fig. 1 as a dashed-dotted line. The agreement with the numerical data is strikingly better, especially for lower J values. The second prediction of Minnhagen's equation is rather more controversial. He finds that above a critical coupling $K_c \approx 1.1$ (or above a critical density) the jump in the helicity modulus is no longer universal. He suggests that this might in particular be seen in the context of frustrated XY models [24]. We will come back to this point at the end of this section where we discuss the numerical results for the jump in the helicity modulus in the present model.

For negative J values, the KT and Ising transitions coincide within the numerical precision. Following this transition line to higher K values, we did not yet observe a KT transition of the fractional charges separately from the Ising transition. If these transitions occur at all distinct from each other, it will probably be impossible to see this, because of the fact that the Ising transition line approaches the line $J = -\pi^2 K/(32\sqrt{2})$, heavy drawn, where one expects a completely different behavior of the system [see Eq. (7)].

It is a striking fact that the point where the Ising and KT transition lines meet, seems to lie at, or very close to, the line $J = 0$, corresponding to the original nearest neighbour XY model. It is not clear at this point

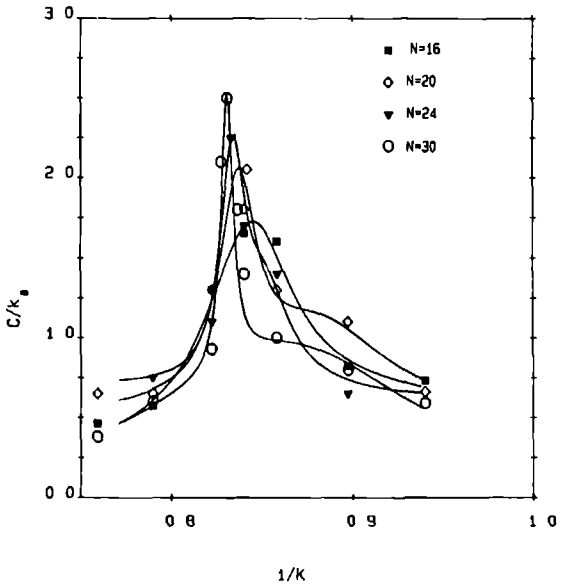

Figure 2: Specific heats at $J = 0$ as a function of K^{-1} for different lattice sizes. The drawn curves are a guide to the eye.

if a special symmetry in the original model is responsible for this fact, also found by Granato [12] in a renormalization study of a model that takes only integer vortices into account (Sec. 1). The coincidence of the transitions in the original model is confirmed by other numerical work [1-4], even if the neirest neighbour cosine interaction is changed into a different shape [5, 6]. Also Berge *et al.* [7] find both transitions coinciding in the original model (corresponding to $\eta = 1$) and separated transitions for $\eta \neq 1$. However, their modification of the model does not correspond to an extra wall energy, but to an alteration of the symmetry of the model, as has already been noted in Sec. 1.

To check if the two transitions coincide indeed at $J = 0$, we have performed a finite size scaling analysis (Fig. 2–4). The peak positions of the specific heat are represented in the upper part of Fig. 3 versus L^{-1}. From this figure, one finds the Ising transition at $K = 1.22 \pm 0.01$. The KT

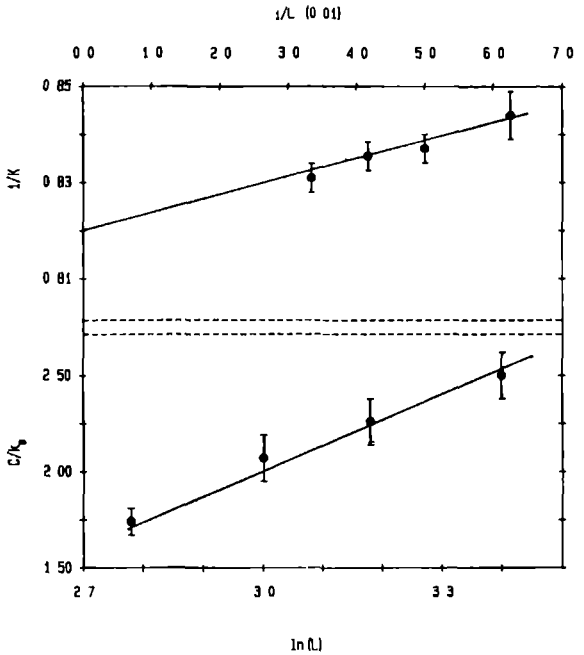

Figure 3: Peak heights of the specific heat (upper part) and peak positions as a function of L (lower part) for $J = 0$.

transition is located at 1.21 ± 0.01 where the KT transition was determined by the condition that the finite size dependence of Υ should be maximal there. So, within the numerical accuracy, the two transitions coincide at $J = 0$.

The peak heights of the specific heat at $J = 0$ are drawn in the lower part of Fig. 3 as a funcion of $\ln N$. Logarithmic behavior, characteristic for Ising transitions, is compatible with the results.

The jump in the helicity modulus at $J = 0$ is within numerical precision in accordance with the universal value of the KT theory (see Fig. 4). The nonuniversal value predicted by Minnhagen (also shown in Fig. 4) is at this point too close to the universal value to be able to discriminate between the two.

To check Minnhagen's prediction we performed a finite size analysis for the helicity modulus at $J = -0.12$. One finds that the jump is nonuniversal

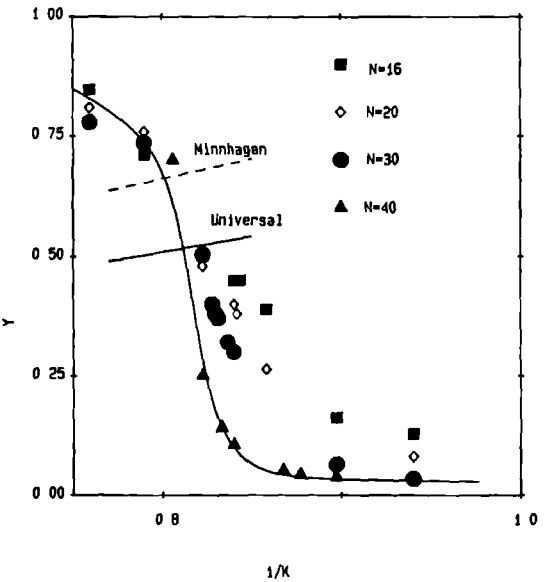

Figure 4: Helicity modulus as a function of K^{-1} at $J = 0$ for different lattice sizes. The drawn curve is a guide to the eye.

and roughly of the size predicted by Minnhagen. However, one should realize that the larger value of the jump in this region can also be explained by a completely different mechanism, namely the unbinding of the fractional charges triggered by the Ising transition (Sec. 3). In favor of this latter explanation is the rather peculiar finite size behavior found for the helicity modulus. As can be seen from Fig. 5, the graphs drawn for the various lattice sizes intersect in contrast to what is usually found for a KT transition (compare e.g. Fig. 4). This is caused by the fact that the helicity modulus *decreases* with the lattice size when coming from the low temperature (high K) side and increases for lower K values. This result can be explained, when the transition is triggered by the Ising transition, because the fractional charges unbind earlier due to the fact that the Ising transition is smeared out as the lattice size diminishes.

The results presented here are far from being conclusive with respect to

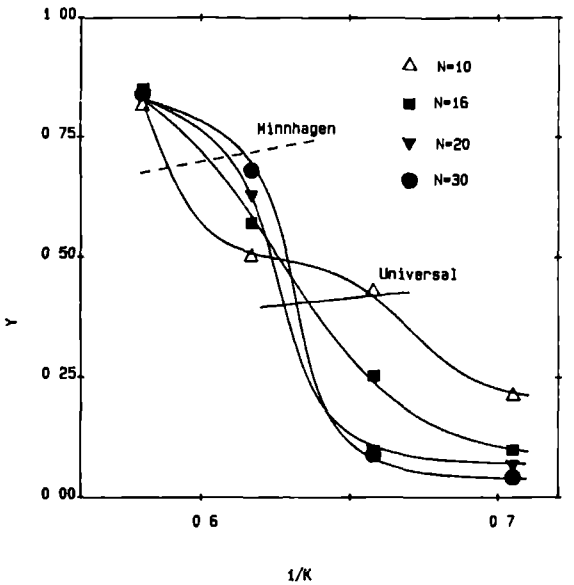

Figure 5: Helicity Modulus as a function of K^{-1} at $J = -0\ 12$ for different lattice sizes Drawn curves are a guide to the eye

the nature of the transition. However, it is clear that one should be careful in explaining nonuniversal jumps in frustrated XY models. Minnhagens prediction should therefore better be tested in a Coulomb gas with integer charges only at a small chemical potential.

Acknowledgements

We Thank Dr. T. Janssen and Dr. J. van Himbergen for useful discussions. This work is part of the research program of the Stichting voor Fundamenteel Onderzoek der Materie (Foundation of Fundamental research on Matter) and was made possible by financial support from the Nederlandse Organisatie voor Zuiver Wetenschappelijk Onderzoek (Netherlands Foundation for the Advancement of Pure Research).

References

[1] S. Miyashita and H. Shiba, J. Phys. Soc. Jpn **53**, 1145 (1984).

[2] S. Teitel and C. Jayaprakash, Phys. Rev. B **27**, 598 (1983).

[3] D.H. Lee, J.D. Joannopoulos, J.W. Negele and D.P. Landau, Phys. Rev. B **33**, 450 (1986).

[4] H. Lee, J.D. Joannopoulos, J.W. Negele and D.P. Landau, Jetp. Letter. **43**, 66 (1986).

[5] J.E. van Himbergen, Phys. Rev. B **33**, 7857 (1986).

[6] J.E. van Himbergen, Phys. Rev. B **34**, 6567 (1986).

[7] B. Berge, H. Diep, A. Ghazali and P. Lallemand, Phys. Rev. B **34**, 3177 (1986).

[8] S.E. Korshunov and G.V. Uimin, J. Stat. Phys. **43**, 1 (1986).

[9] S.E. Korshunov, J. Stat. Phys. **43**, 17 (1986).

[10] E. Granato, J.M. Kosterlitz and J. Poulter, Phys. Rev. B **33**, 4767 (1986).

[11] M.Y. Choi and S. Doniach, Phys. Rev. B **31**, 4516 (1985).

[12] E.Granato, J. Phys. C **20**, L215 (1987).

[13] T.C. Halsey, J. Phys. C **18**, 2437 (1985).

[14] M. Kardar, Phys. Rev. B **33**, 3125 (1986).

[15] B.J. van Wees, H.S.J. van der Zant, and J.E. Mooy, Phys. Rev. B **35**, 7291 (1987).

[16] J.M. Kosterlitz and D. Thouless, J. Phys. C **6**, 1181 (1973).

[17] J.V. José, L.P. Kadanoff, S. Kirkpatrick and D.R. Nelson, Phys. Rev. B **16**, 1217 (1977).

[18] J.E. van Himbergen and S. Chakravarty, Phys. Rev. B **23**, 359 (1981).

[19] T. Ohta and J.D. Jasnow, Phys. Rev. B **20**, 139 (1979).

[20] Y. Saito and H. Müller-Krumbhaar, Phys. Rev. B **23**, 308 (1981).

[21] L.P. Kadanoff, Phys. Rev. Lett. **23**, 1430 (1969).

[22] P. Minnhagen, Phys. Rev. B **32**, 3088 (1985).

[23] P. Minnhagen, Phys. Rev. B **32**, 7548 (1985).

[24] P. Minnhagen, Phys. Rev. Lett. **54**, 2351 (1985).

[25] D.J. Amit, Y.Y. GoldSchmidt, and G. Grinstein, J. Phys A **13**, 585 (1980).

Chapter 5

Phase diagram of the frustrated XY model on a triangular lattice

We formulate a Coulomb gas (CG) model consisting of fractional charges $\pm\frac{1}{2}$ on a honeycomb lattice, representing a frustrated XY model on a triangular lattice. An Ising interaction with coupling constant J is added to this Coulomb gas so as to be able to vary the Ising domain wall energy independently from the Coulomb gas coupling K. In this model, we find Kosterlitz-Thouless (KT) and Ising transitions at separate temperatures for positive J. The point in the phase diagram of this model where the Ising and Kosterlitz-Thouless transition lines meet, has negative J, in contrast to a similar model on a square lattice, that was studied in a previous paper, where the transition lines merge at $J = 0$, corresponding to the "pure" frustrated XY model. For larger K-values (and more negative J), both transitions continue as a single line. Arguments have been given for this line to bifurcate again in the honeycomb CG at very large K. This was not observed, as the system switches over to a different ground state, thus inducing a first order transition.

Published in Phys. Rev. B **40**, 5211 (1989).

In recent years, frustrated XY models have been studied by analytical and numerical methods because of their relevance to arrays of coupled Josephson junctions in a transverse magnetic field [1]. On a triangular lattice, such a model is realized in the antiferromagnetic planar (AFP) model:

$$\frac{1}{kT}\mathcal{H}_{AFP} = -K \sum_{<i,j>} \cos(\phi_i - \phi_j) \tag{1}$$

where the sum is over all nearest neighbour sites of the triangular lattice.

Frustrated XY models combine an Ising $\mathbf{Z}_2$ symmetry [the model defined in Eq. (1) has a twofold degenerate ground state, in each of which nearest neighbour spins have a mutual angle of 120°] with a rotational $U(1)$ symmetry, and based on this observation, one expects an Ising transition and a Kosterlitz-Thouless (KT) transition to occur. Such transitions have indeed been found in numerical simulations on the triangular and square lattice [2-5]. Furthermore, they appeared to occur simultaneously in both cases.

Several authors [5-8] have tried to modify the XY Hamiltonian to observe the two transitions separately at different temperatures. Granato, Kosterlitz and Poulter [6] use a Landau-Ginsburg version of the frustrated XY Hamiltonian, which they believe to be in the same universality class, but which lacks fractional vortices (see below). They find, by renormalization group analysis, a phase diagram in which the KT transition either precedes the Ising transition on raising the temperature or coincides with it. A qualitatively similar phase diagram was found in Monte Carlo (MC) simulations by Berge *et al.* [7] and Eikmans *et al.* [8], who altered the translation symmetry of the original model on a square lattice. van Himbergen [5] tried to separate the transitions in the AFP model on the triangular lattice by adding higher harmonics to the cosine interaction in Eq. (1). He found coinciding transitions for several types of interactions. However, it turned out that this method left only a relatively narrow room for variation, as adding higher harmonics soon leads to a change in the ground state structure.

Another modification of the frustrated model on a square lattice, was suggested by Thijssen and Knops in a recent paper [9].

First, the model was translated by an exact mapping on a Coulomb gas consisting of $\pm\frac{1}{2}$ charges, centered on the faces of the lattice and forming a checkerboard ground state. An Ising nearest neighbour interaction with

coupling constant J was then added, so that the domain wall energy could be varied independently from the CG coupling constant K. To obtain a better understanding of the behavior of the system, one considers instead of the charges on the lattice faces, new charges at the sites of the original lattice, that are equal to the average of the four neighbouring charges, so as to make the ground state neutral. The excitations now consist of Ising domain walls with fractional charges of strength $\pm\frac{1}{4}$ at the corners of these walls.

MC simulations confirmed the prediction by Korshunov [10] and Halsey [11]: If the Ising coupling constant J is large, one finds an Ising transition occurring at a higher temperature than the KT transition. These two transitions then merge within numerical precision at $J = 0$, and continue as a single transition line for $J < 0$. Along this line, the Ising transition triggers the proliferation of free fractional charges, because the domain walls connecting these charges lose their tension at the transition. It is not clear at this moment wether the location of the bifurcation point at $J = 0$ is a mere coincidence or wether it has a deeper reason; however, see Ref. 12.

At still lower values of J, the Coulomb coupling strength K becomes so large at the transition, that one may expect it to be strong enough to keep the fractional charges bound when the walls melt. In that case, the Ising transition will be into a KT ordered phase, so that the two transitions are again separated, but now in reverse order. However, as Korshunov [13] pointed out to us, for the square lattice, the two transition lines, if distinct at all, will be very close to each other in this region of the phase diagram. The reason for this is the following: the only wall excitations in the intermediate region, are those in which they form kinks, i.e. if a wall runs in, say, a vertical direction, it can have only *small* horizontal excursions of length $2, 4, 6 \ldots$ (for odd lengths between two corners, the corresponding fractional charges are equal), because the fractional charges only occur in bound dipole pairs. The walls thus have so small an entropy, that the wall energy (i.e. the energy per unit length of a straight domain wall) must be almost equal to zero, to have zero wall tension. A vanishing wall energy will invoke a proliferation of walls in the ground state and therefore a different ground state structure, so that the analysis presented here, is no more valid. If the Ising transition is then so close to the boundary in the phase diagram beyond which one has a completely different behavior, it will be impossible to observe a KT

transition between them in a MC simulation.

On the triangular lattice, the situation is different [13]. In this case, domain walls can make turns (namely of 120 and 240°), that do not generate fractional charges at their corners. This gives room for entropy, even for large Coulomb coupling K, so that the Ising transition may come to be well separated from the border line of the antiferromagnetic ground state.

We performed a Monte-Carlo simulation of the CG representation of the frustrated XY model on a triangular lattice, as defined in Eq. (1), but with the cosine interaction replaced by the Villain interaction. This model can be mapped on a Coulomb gas, defined on the honeycomb lattice, formed by the centres of the faces of the triangular lattice:

$$\begin{aligned} -\frac{1}{kT}\mathcal{H} &= \frac{1}{2}K \sum_{\mathbf{R},\mathbf{R}'} m(\mathbf{R})m(\mathbf{R}')V(\mathbf{R}-\mathbf{R}') \\ &\quad -J \sum_{<\mathbf{R},\mathbf{R}'>} m(\mathbf{R})m(\mathbf{R}') \end{aligned} \tag{2}$$

where we have included the extra Ising term as was done in Ref. 9. The charges $m(\mathbf{R})$ take on the values $\pm\frac{1}{2}$. $V(\mathbf{R})$ is the lattice Green function with logarithmic long range behavior (see below).

Motivation for this work was first to see if it is indeed possible in this case to find the second bifurcation for strongly negative J and large K. Second, we were interested to see wether the first bifurcation point (at a small K-value), is again located at $J = 0$. When mapping the AFP model on a triangular lattice on a Coulomb gas, one has to consider the honeycomb lattice as a regular lattice with basis vectors $\mathbf{a}_1 = (1,0); \mathbf{a}_2 = (1/2, 1/2\sqrt{3})$ with two sites, A and B in each cell as in Fig. 1.

The lattice Green's function consists of four functions $V^{(ij)}$, $i,j = A,B$ for the interaction between the i- and j-sites:

$$\begin{aligned} V^{(AA)}(\mathbf{R}) &= V^{(BB)}(\mathbf{R}) = \\ &\frac{2}{N^2}\sum_{\mathbf{q}\neq\mathbf{0}} \frac{1-e^{i\mathbf{qR}}}{\frac{2}{3}\{3-\cos(\mathbf{qa_1})-\cos(\mathbf{qa_2})-\cos[\mathbf{q}(\mathbf{a_1}-\mathbf{a_2})]\}} \\ V^{(AB)}(\mathbf{R}) &= V^{(BA)*}(\mathbf{R}) = \\ &\frac{2}{N^2}\sum_{\mathbf{q}\neq\mathbf{0}} \frac{1-e^{i\mathbf{qR}}\frac{1}{3}(1+e^{i\mathbf{qa}_1}+e^{i\mathbf{qa}_2})}{\frac{2}{3}\{3-\cos(\mathbf{qa_1})-\cos(\mathbf{qa_2})-\cos[\mathbf{q}(\mathbf{a_1}-\mathbf{a_2})]\}} \end{aligned}$$

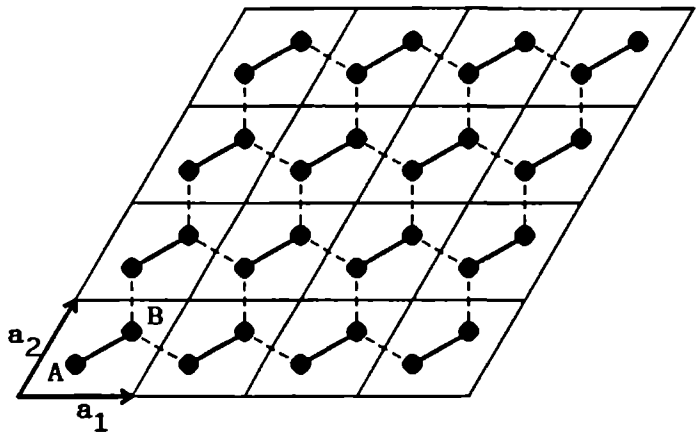

Figure 1: The honeycomb lattice viewed as a regular lattice with a basis. Each cell of the regular lattice contains two sites of the honeycomb lattice, A and B.

(3)

The long range behavior of these potentials is

$$\lim_{R\to\infty} V(\mathbf{R}) = \frac{\sqrt{3}}{\pi}[\ln(R) + 1.815] \tag{4}$$

where the constant 1.815 is determined numerically.

The dielectric constant measures the effect of screening in the Coulomb gas. One calculates it by introducing infinitesimal charges α and $-\alpha$ in the system and then determining the screened potential V_s. If α and $-\alpha$ are both placed on A-sites, the screened potential is

$$V_s^{(AA)} = \frac{1}{2}\frac{\partial^2}{\partial\alpha^2}\ln Z(\alpha) \tag{5}$$

where $Z(\alpha)$ is the partition function with the charges α and $-\alpha$ present.

Expanding in α, we get for the AA interaction:

$$\lim_{q\to 0}\frac{1}{\epsilon_{\mathbf{q}}^{AA}} = 1 \quad - \quad g^{(AA)}(\mathbf{q})V^{(AA)}(\mathbf{q})$$

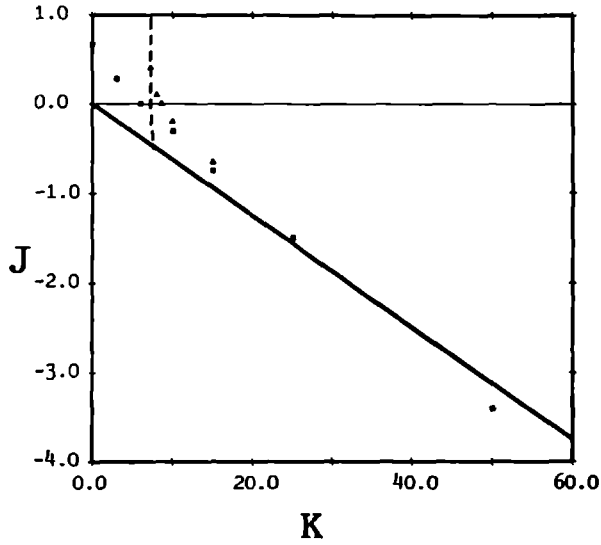

Figure 2: Phase diagram of the honeycomb CG as defined in Eq. 2. Solid squares denote Ising transition points and solid triangles KT points. The heavy line marks the cross over from the antiferromagnetic to the layered ground state. The dashed line is the theoretical KT line for low charge densities, determined by Eq. 7.

$$\begin{aligned} &- g^{(AB)}(\mathbf{q})V^{(BA)}(\mathbf{q}) - g^{(BA)}(\mathbf{q})V^{(AB)}(\mathbf{q}) \\ &- g^{(BB)}(\mathbf{q})V^{(BA)}(\mathbf{q})V^{(AB)}(\mathbf{q})/V^{(AA)}(\mathbf{q}) \end{aligned} \tag{6}$$

where, in the right hand side, $\mathbf{q}$ should be taken to be $\mathbf{q} = \mathbf{K}_1/N$ where $\mathbf{K}_1$ is the first reciprocal vector of the regular lattice: $\mathbf{K}_1 = \frac{4\pi}{\sqrt{3}}(\frac{1}{2}\sqrt{3}, -\frac{1}{2})$.

The (inverse) dielectric constant was used, as usual, to determine the locus of the KT transition, where it drops to zero with a universal jump when the KT transition is distinct from the Ising transition and a jump that can be nonuniversal when the two transitions coincide [9, 14]. The specific heat was measured to determine the Ising transition.

To obtain the global phase diagram, we performed MC simulations for 16×32 and 24×48 lattices. The number of MC steps varied between 10000 and 30000. The resulting phase diagram is represented in Fig. 2. One notes

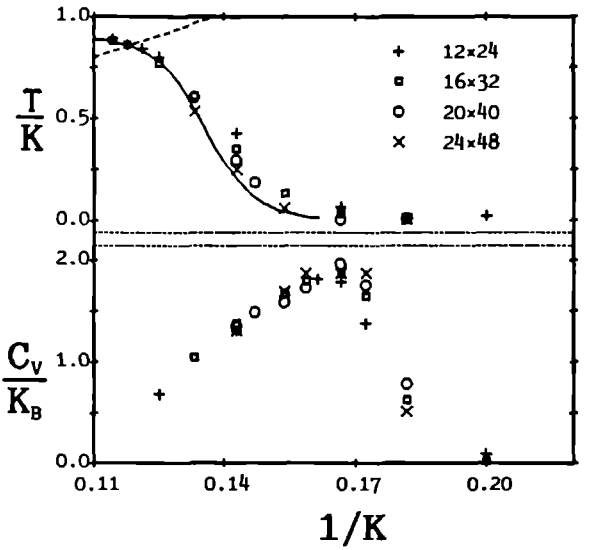

Figure 3: Finite size behavior of the specific heat (lower part) and helicity modulus $\Upsilon/K = \frac{1}{\epsilon}$ (upper part) vs. the CG temperature $1/K$ The dashed line in the upper part represents the universal jump prediction.

the Ising transition line starting at $J \approx 0.66$, $K = 0$, and the KT line, lying in the lower (CG) temperature region. By Eq. (4), the KT line must start off for very large J at K determined by $\frac{\sqrt{3}}{\pi}K = 4$, hence $K \approx 7.25$. If we estimate the fugacity for integer charges as being the energy needed to flip a single spin in the ground state, we get

$$K_c = \frac{4\pi}{\sqrt{3}}\left(1 + 2\pi e^{-6J-\sqrt{3}/\pi \cdot 1.815K}\right) \tag{7}$$

which is represented as the dashed line in Fig. 2. Clearly, the lines do not meet at $J = 0$. The bifurcation point turns out to be located at $K = 28 \pm 2$, $J = -0.7 \pm 0.1$.

Determination of the location of the Ising transition at $J = 0$ is not easy (see Fig. 3). When one does finite size scaling calculations, it turns out that there is a broad maximum of the specific heat at about $K = 6.2$, which shows practically no finite size dependence. This peak is due to the

KT transition and is well known to occur at a somewhat higher temperature than the transition itself. For $K \approx 5.8$, there *is* finite size dependence on the flank of the KT peak, so to do a decent finite size scaling analysis, one should do calculations on much larger lattices, which was not possible, as the computer time increases strongly with the lattice size. On the basis of our results, we can therefore determine the locus of the Ising transition with a moderate precision only: $K_I = 5.8 \pm 0.4$.

The KT transition could be determined more precisely, from the universal value of the jump in the dielectric constant (Fig. 3, upper part). The result is $K_{KT} = 8.6 \pm 0.1$.

The fact that both transitions are sparated at $J = 0$ differs from the situation in the square lattice model, and also from other simulations for the triangular model [4] where the usual cosine interaction was used instead of the Villain interaction, which leads exactly to the Coulomb gas. Apparently, the cosine model has, at the point of the KT transition, a *lower* effective wall energy as compared to the Villain model at its KT transition point (on the line $J = 0$). In the case of the triangular lattice, there is no further direct evidence in support of this conclusion for lack of numerical data on wall energies. However, in the case of the square lattice, where more data are available, the same trend is observed. The wall energy for the Villain model is given by [9] :

$$E_{wall}^{Villain} = \frac{\pi^2}{16\sqrt{2}} K. \tag{8}$$

which at the transition point $K_c = 1.22$ corresponds to $E_{wall}^{Villain} \approx 0.53$.

Halsey [11] finds for the cosine model a wall energy $E_{wall}^{cosine} \approx 0.24K$ (K is the spinwave coupling strength $K = \frac{1}{2}\sqrt{2}\frac{1}{T}$); at the the transition point $K_c = 1.57$ (Ref. 2), this gives $E_{wall}^{cosine} \approx 0.38$.

We now turn to the question of a possible second bifurcation point for large K and strongly negative J. As the fractional charges, that take on values $\pm\frac{1}{4}$, should be logarithmically bound when crossing the Ising transition line, a minimum value for K for the bifurcation to occur is given by $K = 16 \times 4\pi/\sqrt{3} \approx 65$ [see Eq. (4)].

For $K = 50$, 100 and 150, we did not find separate transitions. When the transition occurs at these high K values (where it is first order), we find sometimes even negative values for $\frac{1}{\epsilon}$! The explanation for this, which

is confirmed by inspection of the configurations generated starting from the antiferromagnetic configuration, is that one crosses over to a different ground state. This seems to be in contradiction with what has been said above about the entropy of neutral domain walls. However, there we tested the stability of the antiferromagnetic ground state by considering only the energy of isolated Ising domain walls. By calculating numerically the energies of neutral domain walls, in the honeycomb CG, we estimated this wall energy per unit length to vary between K and $5K$ for long domain walls. This is always far below the joint transition line in Fig. 2. However, if one calculates the energy for a "striped" phase, consisting of alternating rows of + and − charges, $[m_1(\mathbf{R}) = m_2(\mathbf{R}) = (-1)^y]$, one gets

$$E_{striped} = \frac{N^2}{4}K + N^2 J \tag{9}$$

Comparing this with the energy of the antiferromagnetic case, which is equal to

$$-3N^2 J + KV^{(ij)}(\mathbf{k} = \mathbf{0}) = -3N^2 J \tag{10}$$

one gets a borderline given by $K = -16J$, which is well above the borderline determined by zero wall energy.

In the case of the square lattice, the situation is different: the energy of a long straight domain wall can be calculated exactly [Eq. (8)] and the line where this energy vanishes lies *above* the line where the striped phase energy becomes equal to the energy of the antiferromagnetic state.

The transition we find in the triangular model for high K is first order. The line represented in Fig. 2 for $K > 45$, is the line where the transition occurs when starting with the antiferromagnetic configuration and corresponds to the line at which the energy needed to flip two charges in the antiferromagnetic state becomes smaller than approximately 10.

When starting form the striped phase, one flips over to the antiferromagnetic phase at positive J. We find thus a very strong hysteresis, which is characteristic for first-order transitions.

We thank Dr. H.J.F. Knops for useful discussions. This work is part of the research program of the Stichting voor Fundamenteel Onderzoek der Materie (Foundation of Fundamental Research on Matter) and was made

possible by financial support from the Nederlandse Organisatie voor Zuiver Wetenschappelijk Onderzoek (Netherlands Foundation for the advancement of Pure Research).

References

[1] See, for example, *Proceedings of the NATO Advanced Research Workshop on Coherence in Superconducting Networks, Delft, 1987* [Physica B **152**, (1988)].

[2] S. Teitel and C. Jayaprakash, Phys. Rev. B **27**, 598 (1983).

[3] D.H. Lee, J.D. Joannopoulos, J.W. Negele and D.P. Landau, Phys. Rev. B **33**, 450 (1986).

[4] S. Miyashita and H. Shiba, J. Phys. Soc. Jpn. **53**, 1145 (1984).

[5] J.E. van Himbergen, Phys. Rev. B **33**, 7857 (1986); *ibid.*, **34**, 6567 (1986).

[6] E. Granato, J.M. Kosterlitz and J. Poulter, Phys. Rev. B **33**, 4767 (1986).

[7] B. Berge, H. Diep, A. Ghazali and P. Lallemand, Phys. Rev. B **34**, 3177 (1986).

[8] H. Eikmans, J.E. van Himbergen, H.J.F. Knops and J.M. Thijssen, Phys. Rev. B **39**, 1759 (1989).

[9] J.M. Thijssen and H.J.F. Knops, Phys. Rev. B **37**, 7738, (1988).

[10] S.E. Korshunov and G.V. Uimin, J. Stat. Phys. **43**, 1 (1986); S.E. Korshunov, *ibid.* **43**, 17 (1986).

[11] T.C. Halsey, J. Phys. C **18**, 2437 (1985).

[12] O. Foda, Nucl. Phys. B **300**, 611 (1988).

[13] S.E. Korshunov, private communication.

[14] P. Minnhagen, Phys. Rev. B **32**, 7548 (1985).

Chapter 6

Monte Carlo transfer matrix study of frustrated XY models

We discuss the critical behavior of several models, all related to the nineteen-vertex model. These models combine Ising and Gaussian degrees of freedom and have central charge $c = 3/2$ at the critical point. We present arguments why the frustrated XY model, that also has Gaussian and Ising degrees of freedom, might fall into a different universality class. We use the Monte Carlo transfer matrix method of Blöte and Nightingale to obtain accurate numerical results for the central charge and exponents of the frustrated XY model. In particular, we test the prediction for the central charge c to be equal to $3/2$ also in this model. We find $c = 1.66 \pm 0.04$ for the central charge of the frustrated XY model at the critical point. It is not clear at this stage, to which universality class this critical behavior belongs.

Submitted to Phys. Rev. B

6.1 Introduction

Over the last six years, several papers on 2D fully frustrated XY (FFXY) models have appeared [1-10]. These models represent the statistical properties of 2D arrays of superconducting islands coupled by Josephson junctions. The Hamiltonian is a function of the phases ϕ of the wavefunctions in the superconducting islands. These phases are coupled by the Josephson interaction:

$$-\frac{\mathcal{H}}{kT} = J \sum_{<\mathbf{r},\mathbf{r}'>} \cos(\phi_{\mathbf{r}} - \phi_{\mathbf{r}'} + A_{\mathbf{r},\mathbf{r}'}) \qquad (1)$$

The sum is over the nearest neighbour sites of a lattice, that will be taken quadratic in this paper. The fixed constants $A_{\mathbf{r},\mathbf{r}'}$ are the result of a magnetic field applied perpendicular to the plane of the junctions. We are interested in magnetic fields such, that $\sum A_{\mathbf{r},\mathbf{r}'} = \pi$. In that case, the ground state is, apart from global rotations, twofold degenerate, corresponding to the degeneracy of the antiferromagnetic Ising model. The Ising spins are, in this case, the vorticities residing on the faces of the lattice; in the ground state, these take on the values $\pm\pi$. The restriction on the $A_{\mathbf{r},\mathbf{r}'}$ can be satisfied in various ways, this freedom reflects the gauge freedom of the vector potential of the magnetic field. We will use a gauge in which the $A_{\mathbf{r},\mathbf{r}'}$ are equal to π on alternate columns of the lattice [1, 2].

The FFXY model can be mapped on a Coulomb gas (CG). The vortices show then up as charges $\pm 1/2$ on the sites of the dual lattice. In the ground state, these charges are ordered in an antiferromagnetic pattern. Flipping a charge in this pattern is like creating locally a charge ± 1 with respect to the neutral antiferromagnetic background. Ising domain walls between the two different antiferromagnetic phases carry charges only at their corners, that are surrounded by e.g. one $+1/2$ and three $-1/2$ charges, thus creating a net charge $-1/4$. In fact, a single flipped charge $+1$ can be regarded as four $1/4$ charges at the corners of the domain wall surrounding it. This CG picture of Ising walls with Coulombic charges at their corners is very helpful in understanding the transition mechanisms of the model [2, 5, 6].

As FFXY models combine Ising $\mathbf{Z}_2$ and XY $U(1)$ symmetries, one expects both Ising and Kosterlitz-Thouless (KT) critical behavior. In a previous paper [6], we have analyzed a half-integer CG with an extra Ising coupling between the charges added, so that it becomes possible to tune the

electric interaction and the wall energy independently. We have determined the phase diagram of this model using Monte Carlo methods.

The phase diagram has three branches. For large wall energies, there is a critical line of KT transitions. On raising the temperature, one crosses a second branch, an Ising critical line. These two branches meet and continue as a single critical line. It is believed [6], that on this line, the vanishing of the wall tension at the transition, causes the proliferation of *free* fractional corner charges, triggering the helicity modulus (dielectric constant in the CG) to vanish at the same temperature.

Monte Carlo simulations [1, 7, 8] yield simultaneous occurrence of both transitions on the square and triangular lattice for the model, as defined in Eq. (1). Therefore, this model is believed to correspond to a point somewhere on this joint transition line.

Notwithstanding the coupling between the Ising and the XY degrees of freedom via domain wall corners, one has argued that the transition in the FFXY model maintain a combined Ising-KT character, albeit with a possible nonuniversal jump in the helicity modulus. This view was supported by Monte Carlo simulations consistent with logarithmic dependence of the specific heat on the lattice size, indicating Ising critical behavior.

In the same line of argument, Foda [11] came to the conclusion that at the transition, the model could be described by a single superposition of a critical Ising (= massless Majorana fermion-) and Gaussian (free scalar field) model. This then implies that the model would be one of the simplest supersymmetric systems, with central charge $c = 3/2$, being the sum of the Gaussian ($c = 1$) and Ising ($c = 1/2$) value. The main goal of this paper is then to check this prediction, by calculating the scaling term of the free energy of the model on a strip using the Monte Carlo Transfer Matrix (MCTM) method [12].

We find, surprisingly, $c = 1.66 \pm 0.04$ for the central charge of the FFXY model.

In the next section, we will discuss some models with combined Ising and XY critical behavior, all having $c = 3/2$. In section 3, we will describe, in short, the MCTM method, that has been used here for the first time for the calculation of the central charge of a system with continuous degrees of freedom. In sec. 4, we will present the numerical results for the central charge and some scaling indices of the FFXY model.

6.2 Supersymmetric $c = 3/2$ theories and statistical physics

In string theory, supersymmetry plays a major role [13]. For 2D statistical physics, its significance on the microscopic level is not understood very well. However some of the known statistical models, such as the tricritical Ising model [14], are supersymmetric in the scaling limit.

The simplest class of supersymmetric theories (so-called $N = 1$ supersymmetry) has unitary representations for central charges given by [15]:

$$\begin{aligned} c &= \frac{3}{2}\left[1 - \frac{8}{m(m+2)}\right] \\ &\text{or} \\ c &> 3/2. \end{aligned} \tag{2}$$

The boundary point $c = 3/2$ has a trivial realization in a decoupled Gaussian and critical Ising system:

$$Z(c = 3/2) = Z_{XY}(g) \cdot Z_{Ising}^{crit} \tag{3}$$

It can be shown [16] that the partition function on the torus of the XY model in the critical phase can be written as:

$$Z_{XY} = \sum_{M,M'} Z_{M,M'}(\tilde{g}) \tag{4}$$

where $Z_{M,M'}$ is a Gaussian partition function with two seams $2\pi M$ and $2\pi M'$ across the non-contractible loops around the torus. $\tilde{g}$ is the renormalized coupling constant. The seams form the signature of the periodic nature of XY variables $\phi_{\mathbf{r}}$ left after renormalization.

In the same way, the various $c = 3/2$ models leave their trace in various types of couplings via boundary conditions (BC). If one postulates modular invariance, the number of possible partition functions is restricted. Dixon *et al.* [17] have classified all possible $c = 3/2$ modular invariant supersymmetric parition functions on the torus by twisting the spins along the two edges according to symmetry operations of the modular invariant Eq. (3). One of these symmetry operations is orbifolding, i.e. connecting ϕ to $-\phi$ across an edge. If one orbifolds a Gaussian model, one gets the critical line of the Ashkin Teller model. As orbifold structure is not present in the FFXY model, we will leave this symmetry out of the discussion here. We also leave

out isolated points, found by Dixon *et al.*, as partition functions of form Eq. (3) are parametrized by g.

One is then left with two possibilities: either

$$Z_c = \sum_{M,M'} Z^{PP}_{Ising} Z^{Gauss}_{M,M'} \tag{5}$$

with M, M' integer and PP denoting periodic BC in both directions, or

$$Z_{SA} = \sum_{M,M'} [\quad Z^{PP}_{Ising} Z^{Gauss}_{M,M'} \quad + Z^{AP}_{Ising} Z^{Gauss}_{M+1/2,M'} + Z^{PA}_{Ising} Z^{Gauss}_{M,M'+1/2} \quad + Z^{AA}_{Ising} Z^{Gauss}_{M+1/2,M'+1/2}]. \tag{6}$$

A denotes anti-periodic BC. The first one is called the "circle" partition function, the second one "super affine".

We will now examine three statistical models that combine Ising and XY symmetry. All these models are related to the nineteen-vertex model, introduced by Date *et al.* [18] and have central charge $c = 3/2$. We will also identify their partition functions on the torus.

The 19-vertex model is an extension of the six vertex model by allowing, aside from arrows on the links of the square lattice, also zeroes. The zero links form lines that are closed because of the ice rule being valid in this model. These lines are regarded as the Ising walls. The model is related to a height model, by associating jumps π, 0, and $-\pi$ when crossing respectively a right, zero or left pointing arrow. Di Francesco *et al.* give arguments for the model to renormalize to a Gaussian model with an Ising wall structure added to it. For a special set of weights, they noticed that, as it is clear that single Ising walls around non-contractible loops around the torus introduce an extra jump π in the Gaussian variable, the partition function falls in the super affine class. Di Francesco *et al.* [19] verified numerically that indeed for this model $c = 1.5$.

We then turn to a RSOS model, introduced by den Nijs and Rommelse [20]. This model has nearest neighbour (nn) interactions allowing nn spins to differ by 0, ± 1, and next nearest neighbour interactions that give a lower weight for next nn differing by ± 2 than for equal next nearest neighbours. If this next nn interaction is strong enough, all heights will differ at most 1 from an average height h so that the configurations are always flat. The *domain walls* between phases h and $h \pm 1$ may be (i) practically absent, if the

nn interaction strongly favors equal nn heights (this phase is called "RSOS flat") (ii) disordered if the nn interaction is not to much different from zero (disordered flat, or "DOF" phase), and (iii) ordered in a regular lattice if the nn interaction strongly favors steps 1 between nearest neighbours ("BCSOS flat").

Between (ii) and (iii) there is an Ising transition. It lies on a transition line that is parametrized by the nnn coupling. If one now moves on this line by reducing the nnn coupling, the heights melt from flat to rough, and the Ising and KT transition coincide. Accordingly, Rommelse and den Nijs find $c = 1.50$ at this point.

The RSOS model is related to the 19-vertex model, as the latter can be viewed as a height model with nearest neighbour steps 0, ± 1 with a four-point interaction. However, the scaling parts of the partition functions of the two models at the critical point differ, as the boundary conditions for the height- or the vertex representation are not the same. To see this, consider the RSOS model on a torus of size $L \times L'$ with L, L' even. The number of noncontractible Ising walls must be even for both directions and, consequently, the height difference between two sides of the lattice is also even. Therefore, the partition function is of the circle type.

It is worthwhile to notice, that in the RSOS model, the Ising and KT lines *cross* [20]. So, the $c = 3/2$ line in the 19-vertex model, probably lies at the intersection of two crossing critical planes in an extended parameter space, one plane being Ising-, the other KT-like. In the FFXY model, however, as soon as the Ising and KT lines meet, they merge into a single critical line [6]. This is an indication for the fact that, in the FXY model, there is a different and stronger interplay between the Gaussian and Ising degrees of freedom of the model.

Batchelor *et al.* [21] have analyzed a class of models, that are exactly solvable on four branches in the four dimensional parameter space. We will consider the model for $n = 2$, so that the spins are XY-like. In this model, the spins reside on the centres of the *links* of a square lattice with a Boltzmann weight given by

$$W = 1 + \begin{array}{ll} u & (\mathbf{s_1}\cdot\mathbf{s_2} + \mathbf{s_2}\cdot\mathbf{s_3} + \mathbf{s_3}\cdot\mathbf{s_4} + \mathbf{s_4}\cdot\mathbf{s_1}) + v(\mathbf{s_1}\cdot\mathbf{s_3} + \mathbf{s_2}\cdot\mathbf{s_4}) + \\ w & [(\mathbf{s_1}\cdot\mathbf{s_2})\,(\mathbf{s_3}\cdot\mathbf{s_4}) + (\mathbf{s_2}\cdot\mathbf{s_3})\,(\mathbf{s_4}\cdot\mathbf{s_1})] \end{array} \qquad (7)$$

where the $\mathbf{s}_i$ denote XY-spins of length $n = 2$, numbered clockwise around

a plaquette. At the point $w = 1/(3-\sqrt{2})$, $u = 2\sqrt{2}w\cos(3\pi/8)$ and $v = w(\sqrt{2}-1)$, the model happens to be exactly solvable. The finite size behavior at this point, has been studied numerically [22] and the central charge turns out to be $c = 1.5000 \pm 0.0002$.

The model can, for general n, be mapped on an oriented polygon model. A significant difference with polygon models resulting from e.g. Potts models, is the fact that not every lattice bond must carry a polygon link. The model is therefore equivalent to the 19-vertex model [23].

Periodic BC in the spin model, correspond to periodic BC in the polygon model, so the boundary conditions are identical to those in the 19-vertex model. Therefore, the partition function is super-affine.

The FFXY model at the critical point, does not fall into one of the classes found by Dixon *et al.* In this model, the number of non-contractible Ising walls must be even in both directions. However, two Ising walls can generate either a jump 0 or π in the phase, depending on their location [2]. As the compactification radius of the model is 2π, the partition function can neither be circle-like, nor super-affine. This is another indication for the fact that the interplay between Ising and Gaussian degrees of freedom of the model is different from the other models discussed. This motivates our effort to find a direct evaluation of the central charge of the FFXY model.

6.3 The Monte Carlo Transfer matrix method

Transfer matrix methods are an important tool in calculating the central charge c and scaling indices [24]. The transfer matrix of a model on a strip of width L can be written as [25]:

$$\hat{T} = \exp\left[\frac{2\pi}{L}(\hat{L}_0 + \hat{\bar{L}}_0 - c/12)\right] \tag{8}$$

where $\hat{L}_0, \hat{\bar{L}}_0$ are Virasoro operators. Their eigenvalues are the conformal weights $(h, \bar{h})$, so the energy spectrum of the Hamiltonian defined by $\hat{T} = \exp(-\hat{H})$ looks like

$$E = -\frac{2\pi}{L}(h + \bar{h} - c/12) \tag{9}$$

The MCTM method gives information only on the ground state energy. In a system with periodic BC, the ground state is determined by the identity

operator, having $h = \bar{h} = 0$, so in this case we get the well known behavior for the free energy per spin:

$$f = f_0 - \frac{\pi c}{6L^2}. \tag{10}$$

When one changes the boundary condition, the lowest eigenvalue will no longer be determined by the identity operator. So for example, in an Ising model with antiperiodic BC, the lowest weights are $(h, h') = (1/16, 1/16)$, associated with the Ising magnetic operator, so in this case the $L-$ dependent term in f becomes $-\pi\tilde{c}/(6L^2)$, $\tilde{c} = c - 3/2$.

In a Gaussian model

$$\mathcal{H}_{Gauss} = \frac{g}{4\pi} \int d^2r (\nabla\phi(\mathbf{r}))^2 \tag{11}$$

applying a twist $2q\pi$ over the strip causes the ground state energy to be shifted by $\frac{2\pi}{L} g \frac{q^2}{2}$, where g is the coupling constant. We will use various boundary conditions to analyse the FFXY model on a cylinder.

The MCTM method was developed by Blöte and Nightingale [12]. They used it to study the 3D Heisenberg model. The method is based on the Green's function Monte Carlo method [26] for quantum systems.

We have used the MCTM method for the first time to calculate central charges. Normally, for this purpose, systems with continuous degrees of freedom are mapped onto a loop model [27] and analyzed by finite transfer matrix techniques. We did not find such a mapping for the FFXY model. One could of course attempt to analyse the FFXY model by restricting the spins to discrete values $2\pi n/p$, with p large enough. However, a Monte Carlo investigation showed that for $p = 8$, which could perhaps still be tractable by finite matrix methods, the Ising transition takes place at a higher temperature than the KT transition. This modification gives consequently no acces to the study of cooperative effects between the Ising and KT transition. Therefore, the MCTM method seems to be the appropriate tool to analyze the FFXY model on a strip. We will explain this method briefly here.

Consider first a model having a ground state with a unit cell equal to the lattice unit cell, e.g. the Ising or XY model. First, we formulate the transfer matrix. The transfer matrix gives the Boltzmann weights for adding a new spin to the lattice. We use helical boundary conditions (hbc) to get a transfer matrix that is the same for every spin addition [28]. Denoting a lattice column $|s_1, s_2, \ldots, s_L>$ by $|S>$, then, in the case of only

nearest neighbour interactions Ψ, the transfer matrix for adding one spin is determined by:

$$< S'|T|S >= \prod_{2\leq i\leq L} \delta_{s'_i,s_{i-1}} \exp[\Psi(s'_1,s_1)+\Psi(s'_1,s_L)]. \qquad (12)$$

To calculate the largest eigenvalue of the transfer matrix, we use a Monte Carlo algorithm to generate new states out of old ones. We start with a number of R randomly initialized columns $|S^l>$. Every column is given a weight w^l equal to 1. We write

$$< S'|T|S >= D(S)P(S',S) \qquad (13)$$

where $P(S',S)$ is a normalized probability for the addition of a new spin with fixed "old column" S. In a MCTM step, we first realize the addition of new spins to every column according to the transition probability $P(S',S)$ via a Monte Carlo procedure. The weight of every column is multiplied by $D(S^l)/r$, where r is a normalisation constant (see below). We then expand the number of columns by making an identical copy of every column with a weight larger than a treshold value of, say, 2. The two identical columns both get a weight equal to half the weight of the original column. Also, for any pair of columns i and j in the ensemble with both a weight smaller than a lowest treshold (e.g. 0.5), we keep i *or* j in the ensemble with probability $w_i/(w_i+w_j)$ resp. $w_j/(w_i+w_j)$ and give it a weight (w_i+w_j), while throwing the other away. We then restart adding new spins and so on.

The normalisation constant r is adjusted every step such as to keep the number of columns in the ensemble equal to a target number, R_o.

If we denote S^l_t the column number l after t steps, then

$$\Phi_t(S) = \sum_l < S|S^l_t > w^l_t \qquad (14)$$

is an estimate of the t-th iterate of Φ_0 under T. It is an estimate in the sense that it gives a large but finite number of components of the iterated vector, which has in fact an infinite number of components. Furthermore, the method concentrates these points in phase space in those regions where the vector has appreciable values.

To check that Φ_{t+1} is the iterate of Φ_t, note that the average state after adding a spin to a column $|S^l_t>$ is:

$$\overline{|S^l_{t+1}>} = \sum_{S'} P(S',S^l_t)|S'> = \sum_{S'} |S'>< S'|T/D(S^l_t)|S^l_t > \qquad (15)$$

so for the average of Φ_{t+1} we find:

$$r_{t+1}\overline{\Phi_{t+1}(S)} = r_{t+1} < S|\overline{\Phi_{t+1}} >= r_{t+1}\sum_l w^l_{t+1} < S|\overline{S^l_{t+1}} >=< S|T|\Phi > . \tag{16}$$

The highest eigenvalue is obtained as:

$$\lambda_o = \frac{\sum_S \Phi_0(S,t+1)}{\sum_S \Phi(S,t)}. \tag{17}$$

This number is evaluated and averaged over the total number of M steps made in the simulation.

We have tested the method by applying it to the XY model and find $c \approx 1$ in the KT phase. For $T > T_{KT}$, the KT transition temperature, we still find a term c/L^2 in the free energy per spin with $c \approx 1$, for L up to 12, until the temperature is about 50% higher than T_{KT}. Only then the central charges vanishes, indicating the absence of critical behavior. For the XY model one can better locate the transition temperature by measuring the helicity modulus, i.e. the difference in free energy between periodic and anti-periodic BC. We find $T_{KT} = 0.87 \pm 0.02$, to be compared with $T_{KT} = 0.89$ [29].

In the case of the FFXY model, if we choose helical BC, we get a phase mismatch across the strip that depends on the gauge for $A_{\mathbf{r},\mathbf{r}'}$, which always alternates on the lattice columns. To avoid such alternating mismatches, we choose a double helical structure (Fig. 1). Fig. 2 shows the spins of the old column S and the column after spin addition S'. It is clear from this figure, that a column in our ensemble must contain $L+1$ (or even $L+2$) points (see below).

We add at each step two particles to the system because the system has a unit cell consisting of two lattice unit cells.

In order to have an efficient algorithm, it is desirable to formulate the transfer matrix such that when the S-spins have ground state values, $P(S',S)$ has a maximum for the new particles S' in the same ground state. The natural choice (see Fig. 2):

$$P(S',S) = \frac{1}{D(S)}\exp[J\cos(s'_1 - s_1 + \pi) + J\cos(s'_1 - s_{L+1}) + J\cos(s'_2 - s'_1) + J\cos(s'_2 - s_2)] \tag{18}$$

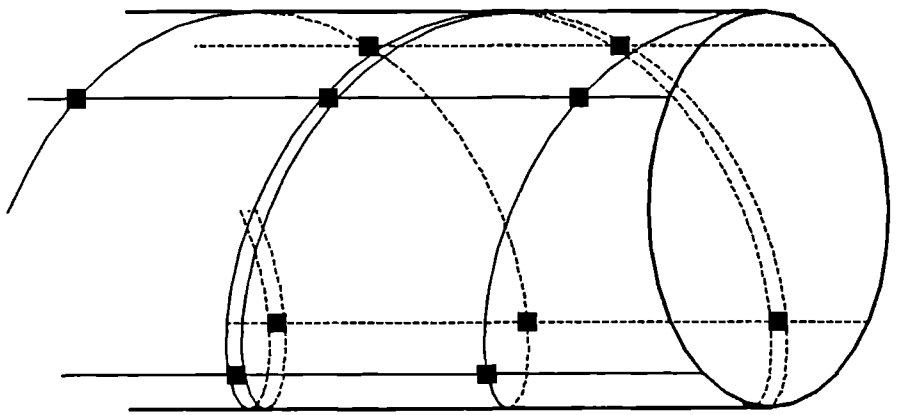

Figure 1: Strip with doubly helical boundary conditions. The double lines represent the bounds for which $A_{\mathbf{r}\,\mathbf{r}'} = \pi$.

with

$$D(S) = \sum_{S,S'} \exp[J\cos(s'_1 - s_1 + \pi) + J\cos(s'_1 - s_{L+1}) + J\cos(s'_2 - s'_1) + J\cos(s'_2 - s_2)] \qquad (19)$$

does not satisfy this criterion and gives bad results, especially for low temperatures, because $P(S', S)$ causes the states in the ensemble to drift away from the ground state.

Therefore, we choose

$$P(S', S) = \frac{1}{D(S)} \sum_{S,S'} \exp[\; J\cos(s'_1 - s_1 + \pi) \;\; +J/2\cos(s'_1 - s_{L+1}) + J/2\cos(s'_2 - s'_1) \;\; +J/2\cos(s'_2 - s_2)] \qquad (20)$$

and the corresponding $D(S)$.

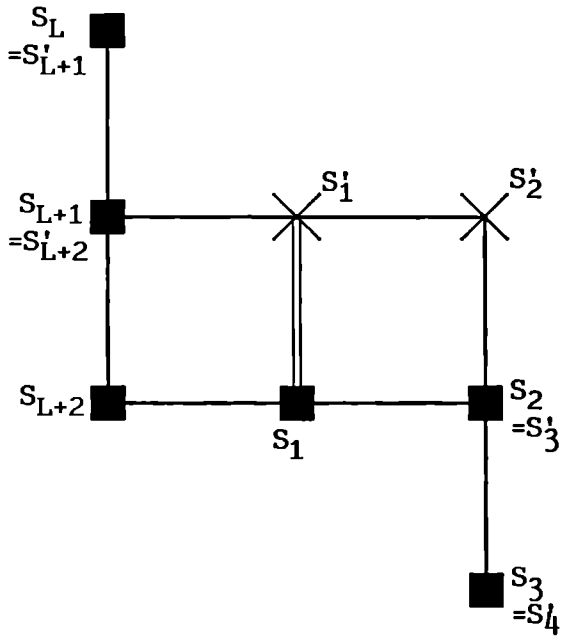

Figure 2: Process of spin addition. The spins s'_i form the new column. The picture shows, that the columns in the ensemble contain $L + 2$ sites, rather than L.

Taking Eq. (18) and (19) instead of Eq. (20), causes the transition temperature to be shifted over 10%. Exponents and central charges remain unaffected by this change. If a spin wave is enforced by applying a jump Δ in the phase ϕ_r across a seam line along the cylinder, the ground state is slightly different. The same holds if one enforces an Ising wall along the cylinder by taking L odd. It is not possible to adjust the method for these boundary conditions. However, as the deviations between the ground state and the maximum of $P(S', S)$ with S fixed in the ground state, are small, we expect this mismatch to have only a small effect on the results. This is confirmed by the fact that, as we will see in the next section, transition temperatures determined with different BC, coincide within numerical precision.

6.4 Numerical results

We have performed extensive MCTM simulations for the FFXY model. To scan the behaviour of the system as a function of temperature we used typically 4000 to 8000 walkers and 8000 to 10000 spin additions. At the transition temperature, to do precise calculations, the number of walkers was 13000, and 14000 spins were added.

To determine the locus of the transition, we determined the point at which the Ising wall energy vanishes. If there is a nonzero wall tension σ, Eq. (10) becomes:

$$f = f_0 - \frac{\sigma}{L} - \frac{\pi c}{6L^2} \tag{21}$$

We first calculated f_0 by extrapolating the results in the absence of an Ising wall (i.e. with even L) to $L \to \infty$. Then, using this value, we fitted data for the system with Ising wall present (odd L) to Eq. (22). In this way one can determine σ.

We carried out this procedure for Ising walls with and without an extra seam $\pi/2$ applied. It should be noted, that in the gauge we use for the $A_{\mathbf{r},\mathbf{r}'}$, an Ising wall induces a jump in the phase of $\pm\pi/2$, where the sign depends on the location of the wall [2]. So, with an extra seam $\pi/2$ applied, there will be a phase mismatch 0 or π on the strip. The results for the wall energy do not differ significantly for the two boundary conditions. The results are presented in Fig. 3. The wall energy clearly falls of linearly with temperature, indicating a thermal scaling index $x_T = 1$. This is in accordance with the results of Teitel and Jayaprakash [1] and Berge *et al.* [4]. Also, the transition point $J = 0.464 \pm 0.05$ is in very good agreement with that of Berge *et al.*, who find $J = 0.465$ for a 30×30 lattice.

As an additional check of the method, we determined the energy per spin as a function of temperature by differentiation of the free energy f. The results, match very well with those of Berge *et al.* for a 20×20 lattice.

The values of the central charge were determined over a range of temperatures, see Fig. 4. At low temperatures, a value $c \approx 1$ is found, but c increases when increasing the temperature. Surprisingly, c rises up to 1.66 ± 0.04 at $T = 0.458 \pm 0.08$. This is in contradiction with the value $3/2$ predicted by Foda [11].

A similar deviation from the supersymmetric models is found in the magnetic exponent x_h, which can be determined by measuring the slope of

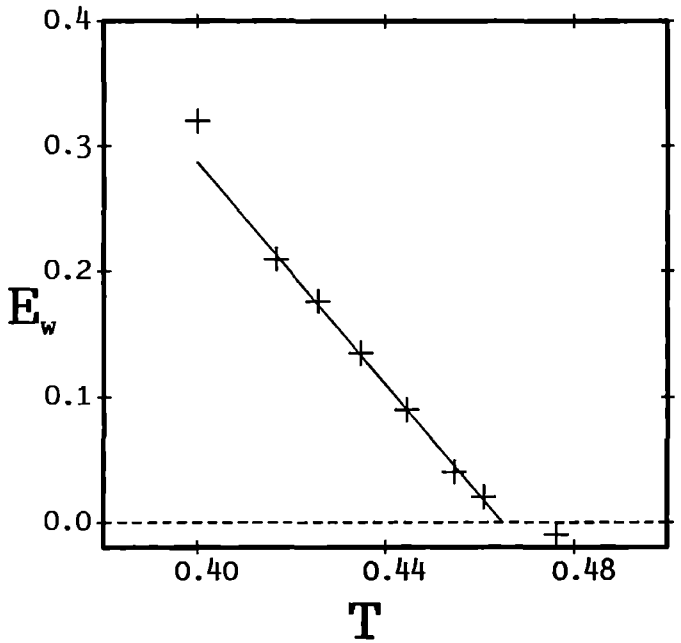

Figure 3: Wall energies as a function of temperature, close to the critical point. The vertical size of the symbols indicate the error. The straight line through the data meets the T-axes at $T = 0.464$.

f as a function of $1/L^2$, which is described by:

$$\tilde{c} = c - 12x_h. \tag{22}$$

If we apply an Ising wall and an extra seam $\pi/2$, which yields, as we have seen above, effectively no phase mismatch, we find $\tilde{c} = -0.72 \pm 0.06$, so that we have $x_h = 0.20 \pm 0.01$ for the magnetic exponent. This clearly differs from the Ising value $x_h = 1/8$.

The helicity modulus, from which one can determine the renormalized Gaussian coupling constant $\tilde{g}$, is determined by applying a seam $2\pi q$ to the even$\times\infty$ strip It has been argued [6], that the jump in the helicity modulus at the transition point may be nonuniversal, because of the fact that the proliferation of free fractional charges at the point where the wall tension vanishes, causes the helicity modulus to vanish, *before* the temperature at

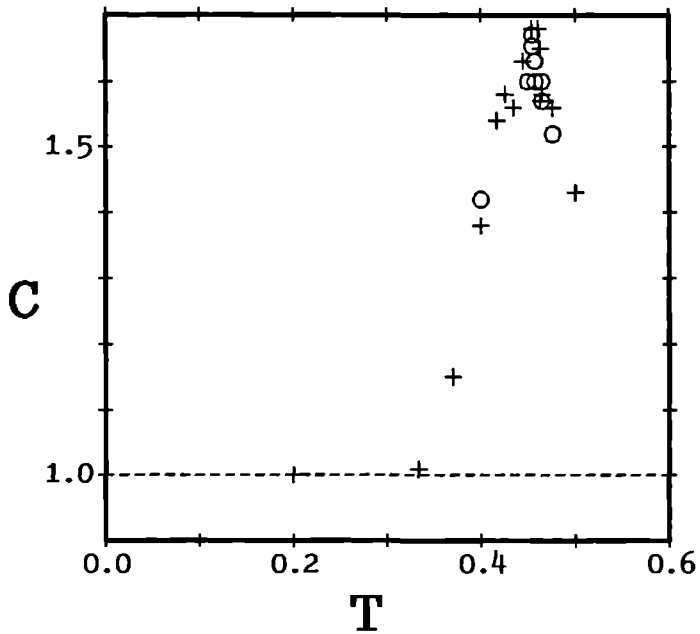

Figure 4: Central charges as a function of the temperature. The open circles denote points calculated with more walkers in the ensemble and more iterations than the plus signs.

which the normal KT transition for integer charges takes place. Monte Carlo simulations give an indication for nonuniversal jumps in various types of XY models [1, 8].

At the transition value $T = 0.464$ we find $\tilde{g} = 4.7$ for $L = 12$ (see Fig. 5), slightly above the universal value $\tilde{g} = 4$. It should however be noticed that (as shown in Fig. 5), there is still a size dependence in the helicity modulus at this point, so that no definite conclusion with respect to the universality of the jump can be drawn.

6.5 Conclusions

The values $c = 1.66 \pm 0.04$, $x_T \approx 1$ and $x_h = 0.22 \pm 0.02$ deviate from what one would expect for a superposition of a Gaussian and Ising model. If the

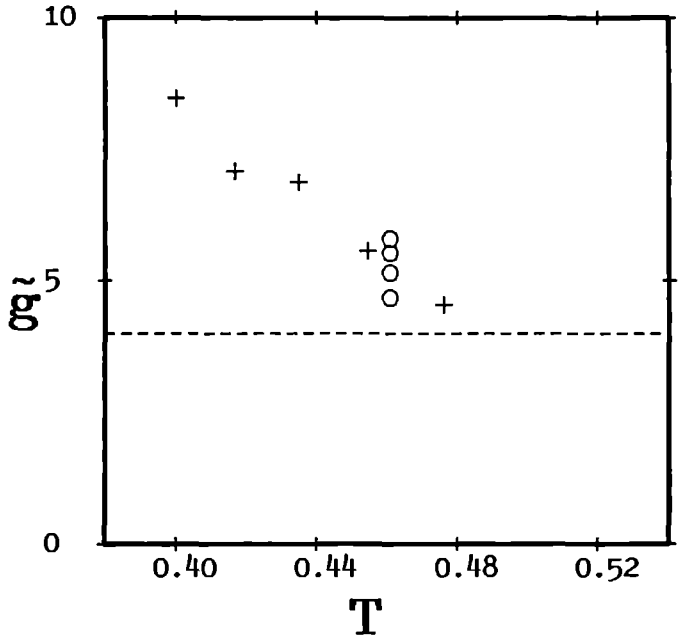

Figure 5: Renormalized coupling constant vs temperature. The circles for $T = 0.465$ represent finite size scaling values. The upper circle corresponds to $L = 6$, the lower to $L = 12$. The + signs are the values for $L = 10$. The dashed line corresponds to the universal value $\tilde{g} = 4$.

model could be described by an Ising system and a XY system (that is, an integer-charge CG), with a relevant coupling between the two, driving the system to a new fixed point, we would expect the central charge to become smaller than 3/2 because of Zamolodchikov's [30] theorem, stating that under renormalization, the central charge of a system can only become smaller. The system of fractional charges must therefore be responsible for the c-value to exceed the value 3/2 and for the deviation of the magnetic exponent from the Ising value.

We have no definite conclusion as to the nature of the critical behavior in the FFXY model. Among the c-values of the minimal unitary supersymmetric series for $N = 1$ and $N = 2$, there is no value that comes close to

1.66.

Acknowledgements

We thank Omar Foda and Henk Blöte for useful discussions. This work was made possible by financial support of the Stichting voor Fundamenteel Onderzoek der Materie (Foundation of Fundamental research of Matter).

References

[1] S. Teitel and C. Jayaprakash, Phys. Rev. B **27**, 598 (1983).

[2] T.C. Halsey, J. Phys. C **18**, 2437 (1985).

[3] D.H. Lee, J.D. Joannopoulos, J.W. Negele and D.P. Landau, Phys.Rev. B **33**, 450 (1986); Jetp. Letter. **43**, 66 (1986).

[4] B. Berge, H. Diep, A. Ghazali and P. Lallemand, Phys. Rev. B **34**, 3177 (1986).

[5] S.E. Korshunov and G.V. Uimin, J. Stat. Phys. **43**, 1 (1986).

[6] J.M. Thijssen and H.J.F. Knops, Phys. Rev. B **37**, 7738, (1988).

[7] S. Miyashita and H. Shiba, J. Phys. Soc. Jpn **53**, 1145 (1984).

[8] J.E. van Himbergen, Phys. Rev. B **33**, 7857 (1986); Phys. Rev. Lett. B **34**, 6567 (1986).

[9] H. Eikmans, J.E. van Himbergen, H.J.F. Knops and J.M. Thijssen Phys. Rev. B **39**, 1759 (1989).

[10] E. Granato, J.M. Kosterlitz and J. Poulter, Phys. Rev. B **33**, 4767 (1986).

[11] O. Foda, Nucl. Phys. B **300**, 611 (1988).

[12] H.W.J. Blöte and M.P. Nightingale Phys. Rev. Lett. **60**, 1562 (1988).

[13] J. Wess and J. Bagger, *Supersymmetry and Supergravity, Princeton Series in Physics*, A.S. Wightman and P.W. Anderson (eds.), Princeton University Press (1983).

[14] D. Friedan, Z. Qiu and S. Shenker, Phys. Lett **151B**, 37 (1985).

[15] D. Friedan, Z. Qiu and S. Shenker, Phys. Rev. Lett. **52**, 1575 (1984); in *Vertex operators in Mathematics and Physics*, edited by J. Lepowski *et al.* (Springer-Verlag, Berlin, 1984); Comm. Math Phys. **107**, 535 (1986).

[16] P. Di Francesco, H. Saleur and J.-B. Zuber, Nucl. Phys. B **280** [FS18], 445 (1987).

[17] L. Dixon, P. Ginsparg and J. Harvey, Nucl. Phys. B **306**, 470 (1988).

[18] E. Date, M. Jimbo, A. Kuniba, T. Miwa and M. Okado, Nucl. Phys. B **290** [FS20], 231 (1987); E. Date, M. Jimbo, T. Miwa and M. Okado, Lett. Math. Phys. **12**, 209 (1986).

[19] P. Di Francesco, H. Saleur and J.-B. Zuber, Nucl. Phys. B **300**, 393 (1988).

[20] M.P.M. den Nijs and K. Rommelse, Phys. Rev. B **40**, 4709 (1989).

[21] M.T. Batchelor, B. Nienhuis and S.O. Warnaar, Phys. Rev. Lett. **62**, 2425 (1989).

[22] H.W.J. Blöte and B. Nienhuis, J. Phys. A **22**, 1415 (1989).

[23] B. Nienhuis, to be published.

[24] H.W.J. Blöte, J.L Cardy and M.P. Nightingale, Phys. Rev. Lett. **56**, 742 (1986).

[25] J. Cardy, Nucl. Phys. B **270** [FS16], 186 (1986).

[26] D.M. Ceperley and M.H. Kalos, in *Monte Carlo Methods in Statistical Physics*, edited by K. Binder (Springer-Verlag, Berlin, 1979).

[27] H.W.J. Blöte and M.P. Nightingale, Physica A **112**, 405 (1982).

[28] It follows from modular invariance, that this boundary condition introduces for spinless ground states in Eq. (10) a correction factor $L^2/(L^2+1)$, which is of no practical importance for the L-values that we use.

[29] P. Minnhagen and H. Weber, Physica B **152**, 50 (1988).

[30] A.B. Zamolodchikov, Pis'ma Zh. Eksp. Teor. Fiz. **43**, 565 (1986).

samenvatting

Fase-overgangen in systemen met gefrustreerde grondtoestanden

In dit proefschrift worden voornamelijk systemen met gefrustreerde grondtoestanden bestudeerd. Deze systemen bestaan uit "spins" op de punten van een rooster. De spins modelleren de microscopische vrijheidsgraden van een thermodynamisch systeem. Zo'n systeem wordt *gefrustreerd* genoemd wanneer de interacties tussen de spins met elkaar in competitie zijn, waardoor in de grondtoestand de afzonderlijke bindingen niet de minimale energie hebben. We zijn met name geinteresseerd in de fase-overgangen die in een dergelijk systeem kunnen optreden. Bij een fase-overgang gaat het systeem van de ene toestand over in de andere, waarbij het verschil tussen de twee toestanden (fasen) vaak gekenmerkt wordt door hun symmetrie: deze symmetrie verandert bij de fase-overgang. Vanuit een fundamenteel oogpunt bezien is de belangstelling vooral gericht op de *continue* fase-overgang, die optreedt op het critische punt waar twee (of meer) fasen identiek worden. Deze critische punten worden gekarakteriseerd door een divergerende correlatielengte. Deze divergentie van de correlatielengte maakt van de ene kant de analyse van het systeem complex door het fundamentele veel-deeltjes

karakter, maar is aan de andere kant ook de basis voor het *universele* gedrag van grote klassen van systemen. Deze universaliteit houdt in dat dat het critisch gedrag van een systeem onveranderd blijft als men details in de interactie verandert, het critisch gedrag blijft binnen dezelfde *universaliteitsklasse*. Een universaliteitsklasse wordt bijvoorbeeld bepaald door de dimensionaliteit van de spin- en roosterruimte en de symmetrie van de resulterende fasen. Het critisch gedrag van een universaliteitsklasse wordt beschreven door een stel getallen, de "critische exponenten": deze getallen karakteriseren de divergentie in thermodynamische grootheden, die het gevolg zijn van de divergerende correlatielengte. Continue fase-overgangen, worden theoretisch geanalyseerd m.b.v. de renormalisatietheorie, die is gebaseerd op het feit dat een critisch systeem invariant is onder schaaltransformaties. In de laatste jaren zijn er belangrijke successen geboekt door de toepassing van de conforme veldentheorie, die een uitbreiding is van de renormalisatietheorie: de schaal-invariantie, die in de renormalisatietheorie op globale schaal gebruikt wordt, wordt hierbij locaal toegepast.

Naast deze theoretische technieken kan men fase-overgangen ook in computersimulaties analyseren, daarvoor gebruikt men de Monte-Carlo techniek of de transfermatrix techniek.

Systemen met frustratie hebben vaak een hoog gedegenereerde grondtoestand. Dit resulteert vaak in ingewikkelde fasediagrammen.

Dat is in het bijzonder het geval in *gemoduleerde* systemen, die als bijzonderheid hebben, dat de structuur van de fase gekenmerkt wordt door een golfvormige modulatie. Bij een fase-overgang in zo'n systeem verandert dan de golflengte van de modulatie. In hoofdstuk 2 bekijken we een voorbeeld van zo'n gemoduleerd systeem, nl. het chirale klok-model. Dit is een model waarbij alle spins drie standen kunnen aannemen en de interacties langs één richting van het d-dimensionale rooster ($d > 2$) zodanig zijn ingericht, dat de fases langs deze richting gemoduleerd zijn. Om het fasediagram van dit model te bepalen, wordt van de Migdal-Kadanoff renormalisatie techniek gebruik gemaakt. Deze techniek was al gebruikt door Huse voor het chirale klok-model, maar in hoofdstuk 2 wordt zijn methode verfijnd door lage temperatuur excitaties op een systematische manier in de vergelijkingen mee te nemen. De resultaten van een lage temperatuurs-expansie voor hetzelfde model door Fisher en Selke worden gereproduceerd, maar de fasen die bij hogere temperatuur op komen zetten worden teveel bepaald door de her-

schalingslengte b (in ons geval $b = 2$) die in de renormalisatie transformatie wordt gebruikt. De structuur van het fasediagram, een zg. "duivelstrap" structuur, die gevonden wordt komt echter wel overeen.

Als voorbereiding op het centrale onderwerp van dit proefschrift, nl. de gefrustreerde XY modellen, wordt in het volgende hoofdstuk een nieuwe theorie voor gewone XY modellen in twee dimensies besproken. De belangrijkste excitaties in dit model zijn vortices, die het karakter hebben van Coulomb ladingen in twee dimensies. De renormalisatietheorie voor het Coulomb gas (CG), die voorgesteld is door Minnhagen, wordt geanalyseerd. Het Coulomb gas bestaat uit positieve en negatieve eenheidsladingen in twee dimensies die via de Coulomb interactie met elkaar wisselwerken. Voor dit gas was in 1974 al een renormalisatietheorie ontwikkeld door Kosterlitz die geldig is voor lage dichtheden, maar Minnhagen heeft in een benadering ook hogere dichtheden willen beschrijven. In het Coulomb gas komt een fase-overgang voor, de zg. Kosterlitz-Thouless (KT) overgang, waarbij de diëlectrische constante van het gas van een universele (d.w.z. onafhankelijk van de dichtheid en van de vorm van de interactie op korte afstand) waarde naar oneindig springt. Het gas gaat dan dus over van een diëlectrische naar een metallische fase. In tegenstelling tot de Kosterlitz renormalisatietheorie, geeft de Minnhagen theorie een niet-universele sprong in de diëlectrische constante en een ander type overgang (eerste orde overgang) als de dichtheid een bepaalde drempelwaarde overschrijdt.

De in hoofdstuk 3 gepresenteerde afleiding is eenvoudiger dan die van Minnhagen en leidt tot vergelijkingen die equivalent zijn aan die van Minnhagen. Onze vergelijkingen hebben echter, in tegenstelling tot die van Minnhagen, de vorm van gewone renormalisatie-vergelijkingen. De niet-universele sprong en het optreden van eerste orde overgangen in het Coulomb gas zijn in de context van deze vergelijkingen het gevolg van het optreden van kruisende trajectorieën, die hier op kunnen treden doordat de randvoorwaarden deels als begin- en deels als eindvoorwaarden van de trajectorieën gegeven zijn. In de gebruikelijke renormalisatietheorie komen uitsluitend beginvoorwaarden voor. Ten slotte stelt deze nieuwe kijk op de vergelijkingen ons in staat om uit twee van zulke trajectoriën een keuze te maken op grond van een fundamenteler criterium, namelijk het minimaal zijn van de vrije energie, dan het *ad hoc* criterium van Minnhagen voor de trajectorie met de langste afschermlengte.

In hoofdstuk 4 komt het hoofdonderwerp van dit proefschrift aan de orde, namelijk fase-overgangen in gefrustreerde XY modellen. Deze modellen zijn varianten van het gewone tweedimensionale XY model, een model waarin de spins vectoren zijn van lengte 1 die in het vlak van het rooster liggen en die een interactie hebben die gelijke naaste-buren spins prefereert. Dit model heeft een fase-overgang van het KT-type, die ook in het Coulomb gas voorkomt.

De interactie tussen de spins wordt anders in de gefrustreerde versie van het model. De frustratie is zodanig, dat in de grondtoestand naast de rotatiesymmetrie van het XY model er een tweevoudige symmetrie ontstaat die ook aanwezig is in het Ising model. Op grond van de twee aanwezige symmetrieën verwacht men zowel Ising- als KT critisch gedrag en de vraag is nu of beide overgangen gescheiden voorkomen en zo ja, in welke volgorde.

Om deze vraag te beantwoorden wordt in hoofdstuk 4 het gefrustreerde XY model op een vierkant rooster afgebeeld op een Coulomb gas dat in dit geval bestaat uit halftallige ladingen (lading 0 komt dus niet voor). Aan de Coulomb interactie tussen deze ladingen wordt een naaste-buren Ising interactie toegevoegd met interactiesterkte J zodat de sterkte van de Ising- en de Coulomb interactie K afzonderlijk ingesteld kunnen worden. Het zo verkregen model kan weer getransformeerd worden in een een model met als excitaties Ising wanden (wanden die de twee mogelijke Ising-fasen scheiden) waarbij op de hoeken van deze wanden ladingen met sterkte $\pm 1/4$ voorkomen, die via de CG interactie met elkaar gekoppeld zijn. Voor dit model is het fasediagram bepaald in een Monte-Carlo simulatie.

Voor positieve J vinden we vinden we gescheiden overgangen met de KT overgang bij een lagere temperatuur dan de Ising overgang. De KT overgang gaat hier samen met een universele sprong in de diëlectrische constante voor heeltallige ladingen (die in het model voorkomen als gesloten Ising-domeinwanden met $4 \times n$ hoekladingen $\pm 1/4$). Voor $J \approx 0$ (geen extra Ising interactie) komen de KT en Ising overgangslijn samen en zetten zij zich voort als één gemeenschappelijke critische lijn voor $J \leq 0$. Langs deze lijn komt de thermische exponent overeen met die van het Ising model. De diëlectrische constante maakt een niet-universele sprong bij het passeren van deze lijn. Dit wordt verklaard doordat het verdwijnen van de vrije energie van de domeinwanden bij de Ising overgang het ontstaan van *vrije* $\pm 1/4$ ladingen mogelijk maakt, waardoor de diëlectrische constante naar oneindig

springt vóórdat de heeltallige ladingen (de gesloten domeinwanden) een KT overgang hebben ondervonden.

Omdat het type rooster van invloed kan zijn op de structuur van het fasediagram wordt in hoofdstuk 5 het gefrustreerde model op een driehoekig rooster aan een soortgelijke analyse onderworpen. Het globale beeld van het fasediagram is gelijk aan dat van het model op een vierkant rooster met dit verschil, dat het punt waar de twee gescheiden overgangslijnen samenvallen, hier gevonden wordt voor $J < 0$. Hoewel er argumenten gegeven zijn voor het opnieuw splitsen van de gemeenschappelijke overgangslijn voor sterk negatieve J, blijkt dit niet het geval te zijn, omdat het systeem in dit gebied van het fasediagram overgaat in een andere grondtoestand, waardoor deze lijn eerste orde wordt.

In het zesde en laatste hoofdstuk gebruiken we de recent ontwikkelde Monte-Carlo transfermatrix (MCTM) techniek om de centrale lading van het gefrustreerde XY model te bepalen. De centrale lading is een getal dat naar voren komt in de conforme veldentheorie. Kennis van de centrale lading van een critisch systeem geeft veel informatie over het critisch gedrag van dat systeem. Voor het gefrustreerde XY model controleren we hiermee de voorspelling dat deze centrale lading c gelijk zou zijn aan 3/2. In dat geval zou het model (met samenvallende Ising- en KT overgang) op het critisch punt beschreven moeten kunnen worden door een Ising model en een Gaussisch model (dit model is equivalent met het XY model bij voor temperaturen beneden de KT overgang) die ongekoppeld zijn. We vinden echter $c = 1.66 \pm 0.04$ op de overgang. In consistentie met dit resultaat vinden we een magnetische exponent die afwijkt van de Ising waarde 1/8. De thermische exponent is echter in overeenstemming met de Ising exponent $x = 1$, dit bevestigt eerder Monte-Carlo werk. Deze resultaten wijzen er dus op dat het critisch gedrag van een andere soort is dan werd verwacht, de aard van de faseovergang in het gefrustreerde XY model is dus nog niet geheel begrepen.

Curriculum vitae

Geboren	27 februari 1958 in Maastricht.
1970–1976	Gymnasium B opleiding aan de scholengemeenschap Jeanne d'Arc te Maastricht.
1976–1983	Doctoraalopleiding theoretische natuurkunde aan de KU Nijmegen.
1982–1984	Werkzaam als docent natuurkunde in het voortgezet onderwijs aan diverse scholen in Nijmegen, Arnhem en Maastricht.
1984–1986	Onderwijsstimuleringsmedewerker aan de KU Nijmegen t.b.v. het project "**C**omputer **A**ssisted **I**nstruction in de sectie natuur- en sterrenkunde".
Vanaf 1986	Werkzaam als promovendus bij FOM beleidsruimte project "Complex phase diagrams with modulated systems" onder begeleiding van dr. T Janssen en dr. H. Knops. Onderwijstaken in deze periode: organisatie en begeleiding bij het gebruik van CAI programma's, verzorgen van diverse werkcolleges en het opzetten van de nieuwe 3^e semester cursus "programmeermethoden", in samenwerking met drs. P. Klok.

Stellingen

1. Methoden om de effectiviteit van Monte Carlo procedures te verbeteren, zoals voorgesteld door Kandel *et al.* en Swendsen en Wang, werken alleen bij discrete spin modellen met korte-drachts wisselwerkingen. Dit houdt een belangrijke beperking in op de toepasbaarheid van zulke methoden.

   R.H. Swendsen en J.S. Wang, Phys. Rev. Lett. **58**, 86 (1987);
   D. Kandel, E. Domany, D. Ron, A. Brandt en E. Loh, Phys. Rev. Lett. **60**, 1591 (1988).

2. De argumenten die in het laatste hoofdstuk van dit proefschrift worden gegeven om de numerieke resultaten voor het gefrustreerde XY model te verklaren, suggereren dat in een gemodificeerd XY model waarin de naaste buren interactie tussen spins ϕ_i en ϕ_j een locaal minimum heeft voor $\phi_i - \phi_j = \pi$, een deel van de critische lijn die correspondeert met de dissociatie van heeltallige vortex paren een centrale lading heeft die groter is dan $3/2$.

   D.H. Lee en G. Grinstein, Phys. Rev. Lett., **55**, 541 (1985).
   S. Korshunov, J. Phys. C **19**, 4427 (1986).

3. Een vruchtbare invalshoek voor het bestuderen van de vraag naar de supergeleidende eigenschappen van materialen zou kunnen zijn om supergeleiding te formuleren als een eis op de golffunctie om, ook in de aanwezigheid van onzuiverheden, geen electrisch dipoolmoment op te kunnen bouwen.

4. Voor een inleidende cursus in het programmeren voor natuurkundestudenten, is Pascal de meest geschikte programmeertaal.

5. De voorbeelden die Kubach noemt om zijn bewering te staven dat overeenkomsten tussen vijf als "pelgrimskerken" bekend staande gebouwen niet met de pelgrimages naar Santiago de Compostella in verband gebracht moeten worden, kunnen ook als argumenten tegen deze bewering aangevoerd worden.

   H.E. Kubach, Romanesque Architecture, Faber & Faber, London, 1988, pag. 118.

6. Het gemiddelde niveau van de stellingen, die gereproduceerd worden op de opiniepagina's van dagbladen, komt niet boven het niveau van deze stelling uit.